Physics of Living Systems

Fragmentation and aggregation of cyanobacterial colonies

Reviewed Preprint
v1 • January 20, 2025
Not revised

Yuri Z Sinzato, Robert Uittenbogaard, Petra M Visser, Jef Huisman, Maziyar Jalaal

Van der Waals-Zeeman Institute, Institute of Physics, University of Amsterdam, Amsterdam, The Netherlands • Hydro-Key Ltd, Haelen, The Netherlands • Department of Freshwater and Marine Ecology, Institute for Biodiversity and Ecosystem Dynamics, University of Amsterdam, Amsterdam, The Netherlands

eLife Assessment

With the goal of investigating the assembly and fragmentation of cellular aggregates, this work investigates cyanobacterial aggregates in a laboratory setting. Investigating the conditions and mechanisms behind aggregation is an **important** contribution as it yields basic understanding of natural processes and offers potential strategies for control. The combination of computational and experimental investigations in this manuscript provides **solid** support for the proposed processes for aggregation and fragmentation, with some concerns about the strength of evidence for a subset of claims.

https://doi.org/10.7554/eLife.103503.1.sa3

Abstract

Fluid flow has a major effect on the aggregation and fragmentation of bacterial colonies. Yet, a generic framework to understand and predict how hydrodynamics affects colony size remains elusive. This study investigates how fluid flow affects the formation and maintenance of large colonial structures in cyanobacteria. We performed experiments on laboratory cultures and lake samples of the cyanobacterium *Microcystis*, while their colony size distribution was measured simultaneously by direct microscopic imaging. We demonstrate that EPS-embedded cells formed by cell division exhibit significant mechanical resistance to shear forces. However, at elevated hydrodynamic stress levels (exceeding those typically generated by surface wind mixing) these colonies experience fragmentation through an erosion process. We also show that single cells can aggregate into small colonies due to fluid flow. However, the structural integrity of these flow-induced colonies is weaker than that of colonies formed by cell division. We provide a mathematical analysis to support the experiments and demonstrate that a population model with two categories of colonies describes the measured size distributions. Our results shed light on the specific conditions wherein flow-induced fragmentation and aggregation of cyanobacteria are decisive and indicate that colony formation under natural conditions is mainly driven by cell division, although flow-induced aggregation could play a role in dense bloom events. These findings can be used to improve prediction models and mitigation strategies for toxic cyanobacterial blooms and also offer potential applications in other areas such as algal biotechnology or medical settings where the dynamics of biological aggregates play a significant role.

Introduction

Many environmental and pathogenic bacteria exhibit colonial forms of life, either as surface biofilms [1, 2] or non-attached aggregates [3–5]. In most situations, these colonies are subjected to hydrodynamic stresses, which may lead to flow-induced fragmentation and aggregation [6]. These physical processes, combined with biological growth, determine the fate of aggregates and the microbial lifestyle. Nonetheless, despite their abundance and fundamental importance, a generic framework to study the effects of fluid flow on bacterial colonies, as well as their fragmentation and aggregation across scales, is still in its infancy [7–10]. Here, we focus on colonies of bloom-forming cyanobacteria and ask the question: how flow-induced aggregation and fragmentation regulate dynamic changes in colony size?

Toxic cyanobacterial blooms are a major nuisance for freshwater ecosystems worldwide [11]. These blooms often lead to increased turbidity, cause harm to other aquatic organisms, and deteriorate water quality. Recent evidence indicates that the severity and frequency of cyanobacterial blooms are increasing due to eutrophication and climate change [12–15]. Consequently, water management authorities show growing interest in techniques to prevent, monitor, and control these toxic blooms [16]. A particular effort is being taken to combat blooms of *Microcystis*, a non-motile colony-forming freshwater cyanobacterial genus that dominates many aquatic ecosystems worldwide [17, 18]. Fluid dynamics is at the heart of *Microcystis* bloom formation, but also on some of the methods to control them. A large colony size and positive buoyancy give *Microcystis* a higher average light dose in comparison to non-buoyant algae [19, 20]. Control methods such as deep artificial mixing can disrupt this competitive advantage by increasing the turbulence level in lakes [21]. Yet, the mechanisms of *Microcystis* colony formation, and in particular, the impact of fluid flow on the formation of colonies are poorly understood.

Microcystis cells are held together by a layer of extracellular polymeric substances (EPS), facilitating the formation of large colonies of up to a millimeter in diameter with diverse morphological arrangements [22–24]. Two main mechanisms for colony formation have been proposed [17]: (i) cell division, *i.e.*, clonal expansion of cells which remain attached by their encapsulating EPS layer after division, and (ii) aggregation, *i.e.*, initially independent cells/colonies collide and adhere to each other. On the one hand, sequencing of the genetic diversity within *Microcystis* colonies supports the hypothesis that colony formation under natural conditions is primarily driven by cell division [25]. On the other hand, cell aggregation can occur on a shorter time scale and may offer improved protection against high grazing pressure [26]. Aggregation becomes significant when the collision frequency is high enough for aggregation rates to overcome cell division rate [6], and the stickiness of colonies is sufficiently large (controlled by the EPS composition, pH, and ionic strength of water or medium [27–29]). In addition to aggregation, fluid flow also influences colony formation through fragmentation, potentially serving as a mechanism for colony reproduction [30] to overcome the growth limitations of large colonies [31]. Beyond modulating colony size through aggregation and fragmentation, fluid flow has also been proposed as a driving factor in changes in colony morphology and growth rate [32–34].

Flow-induced alterations in colony size and morphology impact the vertical migration and grazing resistance of colonies, thereby influencing the success of the *Microcystis* population. This bears significance for forecasting models which have often assumed a fixed colony size [35–37]. Information on colony size is also important for bloom control via artificial mixing systems, which rely on estimates of colony flotation velocity, determined by both colony shape and size [21, 38]. Moreover, it remains uncertain whether mixing systems, such as bubble plumes, can enhance their efficiency by fragmenting colonies or whether artificial mixing may inadvertently

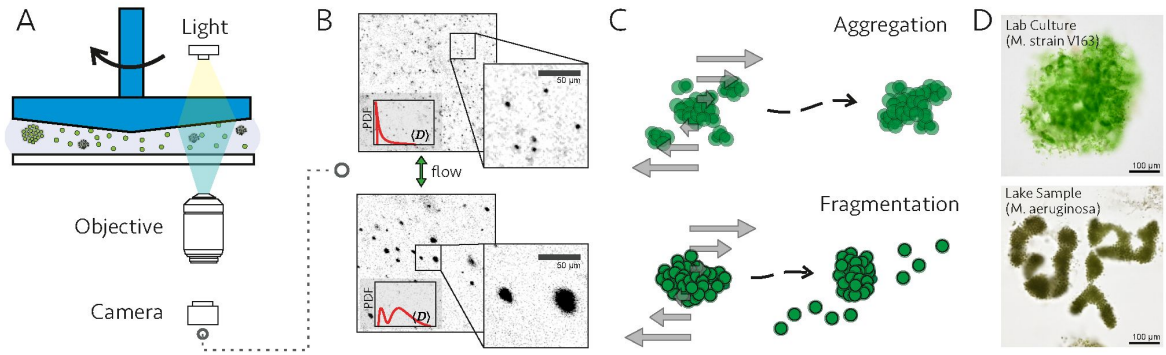

Fig. 1

Methodology used to observe effects of fluid flow on *Microcystis* colonies.

(A) Experimental setup consisting of a (cone- and-plate) controlled flow setup combined with inverted microscopy. The conical upper surface was rotated by a rheometer head, while the stationary glass slide below the sample allowed optical access for the microscope. (B) Examples of microscopy images. Colony size distributions were calculated after image processing of the captured frames. (C) Changes in size distributions (and other complementary measurements) over time were used to identify aggregation and fragmentation of cyanobacterial colonies. (D) The majority of the measurements were conducted using a laboratory culture of *Microcystis* strain V163. Colonies collected from Lake Gaasperplas (Netherlands), dominated by the morphospecies *M. aeruginosa* were also used.

promote aggregation. Colony fragmentation has been observed in grid-stirred [39] and propeller mixed tanks [32] at energy dissipation rates comparable to bubble plumes [40]. However, these studies reported averaged dissipation rates, while local values near the fast moving surfaces can be orders of magnitude higher [41]. Furthermore, the size distribution of the colony fragments has not been characterized.

In the present study, we investigate to what extent *Microcystis* colony fragmentation and/or aggregation occurs at levels of turbulence observed for naturally or artificially mixed lakes. To this end, colonies of a laboratory culture of *Microcystis* were subjected to various intensities of shear flow (**Fig. 1**). We identified the mechanism of colony fragmentation using direct measurements of dynamic changes in colony size distribution under controlled laboratory conditions and analyze the characteristics of colonies formed by aggregation and cell division. Furthermore, the fragmentation behavior of the laboratory culture was compared with field samples of *Microcystis* spp. We also developed a numerical model based on a two-category discrete population to simulate changes in the size of *Microcystis* colonies via aggregation and fragmentation. Finally, we provide a phase map based on flow characteristics and cyanobacterial abundance to highlight different regimes in which fluid flow plays a significant role in cyanobacterial colony formation.

Fragmentation of Large *Microcystis* Colonies Occurs through Erosion

A culture of *Microcystis* strain V163 was filtered to collect large colonies, and colonies on the filter were subsequently re-dispersed in fresh BG-11 medium up to the desired total biovolume fraction φ (*Materials and Methods*). The flow was generated by a cone-and-plate shear operating in an inertial regime, and it was characterized by the average energy dissipation rate $\dot{\varepsilon}$, hereafter called dissipation rate (*Materials and Methods*). The size distribution of the colonies was measured over time by microscopic imaging of the suspension through the transparent lower surface (**Fig. 1**). The colony size is described here by its relative diameter $l = d/d_1$, where d is the Feret's diameter (maximum distance between two boundary points of the colony) and d_1 is the single-cell diameter. The number of cells in a colony, N_c, was calculated from its relative diameter via the relation $N_c = l^f$, where $f = 2.09$ is the average fractal dimension measured for colonies of *Microcystis* strain V163 (*Materials and Methods*). The size distribution was computed as the normalized biovolume distribution $n(l)$, *i.e.*, the number of cells in colonies in size bin $\{l; l + \Delta l\}$, divided by the total number of cells in the suspension.

The results show that the initial size distribution had a bimodal shape, with a subpopulation of small colonies peaking around $l \sim 1 – 2$ (single cells, dimers, and trimers) and a subpopulation of large colonies, peaking around $l \sim 20 – 40$ (**Fig. 2A**). The cut-off size between the two subpopulations is defined here as the minimum of the bimodal distribution. Some small colonies ($l \sim 1 – 2$), up to 20% of the total biovolume, were always present in the initial distribution even after filtration, due to pre-stirring required to keep the suspension homogeneous. However, medium-sized colonies ($l = 4 – 8$) accounted for a negligible fraction of the distribution.

When subjected to an intense dissipation rate ($\dot{\varepsilon} = 5.8\ m^2/s^3$), the large colonies of *Microcystis* strain V163 displayed considerable fragmentation, with their median diameter (50 % percentile of the biovolume distribution of the large colonies) decaying to about half of the initial value after a few hours (**Fig. 2B**). In contrast, the median diameter of small colonies showed little change in size and remained below $l \leq 2$ during the entire experiment. The size distribution after 1 hour indicated that most colonies larger than $l \geq 30$ were fragmented, leading to a rise in the subpopulation of small colonies (**Fig. 2C**). Notably, the bimodal shape of the size distribution was preserved, with very few medium-sized colonies. This suggests that aggregation of single cells into larger colonies is negligible under this intense shear flow condition, and the main effect of the

shear flow on the size distribution is the decrease in size of the large colonies concomitant with an increase in the fraction of small colonies. After a few hours of shear, about 80 % of the total biovolume was composed of small colonies (**Fig. 2D**). This time scale was much shorter than the cell division time, such that changes in the colony size distribution by division could be neglected within the experimental time [20].

Direct measurement of the fragment distribution function $g(l,l')$ (*i.e.*, the frequency of fragments with size l arising from the fragmentation of a colony of size l') is an experimental challenge [42–44]. Individual fragmentation events could not be visualized as the residence time of colonies inside the field of view is too short. Instead, a suitable model can be identified from the rate of change in the biovolume distribution (**Fig. 2E**). A negative rate was observed for large colonies in the range $l \geq 25$, indicating a loss in that size range by fragmentation. In contrast, the newly created fragments appeared as positive peaks, with a distinct peak close to the single-cell size. This result is compatible with an erosion mechanism, in which small fragments with one or a few cells are detached from the outer layer of the colony. For an ideal binary erosion, a fragmentation event of a colony with i cells results in one cell being eroded from the surface of the colony with a complementary fragment of $i-1$ cells remaining. Small deviations from an ideal binary erosion are observed in **Figure 2E**, with most eroded fragments lying in the range $1 \leq l \leq 2$. Nevertheless, ideal erosion provides a good approximation for the results. Accurate identification of complementary fragments from the rate of change in the biovolume distribution was more difficult, because the broad initial distribution of our suspension leaded to a broad distribution of complementary fragments. In this case, the rate of change in the biovolume distribution shifted from a net loss of eroded colonies at larger sizes ($l \geq 25$) to a net gain of complementary fragments at intermediate sizes ($5 \leq l \leq 20$).

Assuming an ideal binary erosion mechanism, the fragmentation frequency $\kappa(l)$ was computed from the temporal dependence of the biovolume distribution (*Materials and Methods*). Here, $\kappa(l)$ is defined as the average number of fragmentation events (loss of a single cell) that one colony of size l suffers per unit of time. The fragmentation frequency of *Microcystis* strain V163 was calculated as a function of colony size for three values of dissipation rate (**Fig. 2F**). The results show that the fragmentation frequency increases with colony size. Furthermore, an increase in dissipation rate sharply intensifies the erosion of colonies, with a two order of magnitude increase in $\kappa(l)$ when $\dot{\varepsilon}$ varies from 1.1 to 9.6 m^2/s^3.

Aggregation-Formed Colonies are Less Resistant than Division-Formed Colonies

In addition to inducing fragmentation, a turbulent flow may also increase the collision frequency of colonies. If the collisions are adhesive and the suspension is concentrated enough, then new colonies will be formed by aggregation. We subjected a single-cell suspension to the cone-and-plate shear flow to investigate whether aggregation can be a dominant colony-forming mechanism compared to cell division. Cultures of the *Microcystis* strain V163 were filtered to obtain a single-cell suspension, and the total biovolume fraction was adjusted with fresh BG-11 medium (*Materials and Methods*). A typical initial bio-volume fraction distribution is presented in **Figure 3A**. In addition to single cells, some small colonies up to $l = 3$ were present in the filtered suspension due to imperfect filtering and/or aggregation during the pre-stirring. The size distribution was unimodal (single peak), in contrast with the bimodal distribution (double peak) in the suspension of division-formed colonies (**Fig. 2A**). After about 1 hour at a moderate dissipation rate ($\dot{\varepsilon} = 0.019\ m^2/s^3$) and a total biovolume fraction of $\varphi = 10^{-4}$, the single-cell suspension showed aggregation of cells into small colonies, with a steady-state median diameter of $l = 1.8$ (**Figs. 3B and 3C**). Note that cell division can be neglected as the measurement time was much shorter than the division time. An increase in the collision rates due to a single-cell

suspension led to an increase in the median diameter, although the increase was minor. At a high total biovolume fraction ($\varphi = 5 \bullet 10^{-4}$), a steady-state median diameter of $l = 2.4$ was reached, with a negligible fraction of colonies above $l \geq 5$ (*SI Appendix*, **Fig. S4C**). Therefore, the aggregation of single cells is likely limited by weak bonds between cells. At the steady-state regime of median diameter, the newly-formed aggregates with a large diameter would be quickly fragmented back into smaller parts.

A suspension of division-formed colonies under the same moderate dissipation rate ($\dot{\varepsilon} = 0.019\ m^2/s^3$) did not suffer noticeable fragmentation (**Fig. 3D**). The culture was grown in quiescent medium, without shaking, thus the colonies are assumed to have formed solely by cell division. The erosion of division-formed colonies was negligible, as the fraction of small colonies remained below 20% (*SI Appendix*, **Fig. S2B**). Furthermore, the nearly constant median diameter of the large colonies (observed also for other total biovolume fraction values, *SI Appendix*, **Fig. S2**) shows that the division-formed colonies did not aggregate at this moderate dissipation rate.

The results above indicate that bonds formed during flow-induced aggregation (whether between two single cells or two division-formed colonies) are weak and cannot withstand intense dissipation rates. In contrast, the bonds between cells within a single division-formed colony are significantly more resistant. This difference in mechanical strength of the cellular binding in aggregation-formed versus division-formed colonies can be attributed to the structure of the EPS layer that surrounds the colonies. Aggregated colonies would have interstices between cells that are not filled with EPS. In contrast, cell division allows enough time for the gaps to be filled with secreted EPS, effectively increasing the bond strength between cells (**Figs. 3B and 3D**). However, we could not confirm this hypothesis visually, as the EPS layer in *Microcystis* strain V163 is too thin (< 1 μm) for a clear identification using optical microscopy.

Dynamical Changes in Colony Size Modeled by a Two-Category Distribution

Our experimental results for colonies of *Microcystis* strain V163 (**Fig. 3**) suggest the presence of two categories of colonies: aggregated colonies (denoted as C_1) and division-formed colonies (C_2). The total biovolume distribution $n(l)$ is given by the sum of both distributions $n_1(l) + n_2(l)$, normalized such that $\int_0^\infty n(l)\,\mathrm{d}l = 1$. Within times shorter than the cell division time, the biovolume distribution of each colony category is described by a population model [27]:

$$\frac{\partial n_i}{\partial t}(l,t) = A_i(l,t) + F_i(l,t) + T_i(l,t)\ , \tag{1}$$

where $A_i(l, t)$ and $F_i(l, t)$ describe the aggregation and fragmentation rates as a function of colony size for each of the two categories, and $T_i(l, t)$ is a transfer rate of biovolume between the two categories. The turbulent shear-induced collisions between colonies shift the distribution towards larger aggregates, and the aggregation rate is given by

$$A_i(l,t) = \frac{6\phi\alpha_i}{\pi}\left[\frac{1}{2}\int_0^l \beta(l',l_o)\left(\frac{l}{l'l_o}\right)^{2f-1} n_i(l',t)\,n_i(l_o,t)\,\mathrm{d}l' - n_i(l,t)\int_0^\infty \beta(l,l')\frac{1}{l'^f}\,n_i(l',t)\,\mathrm{d}l'\right]\ , \tag{2}$$

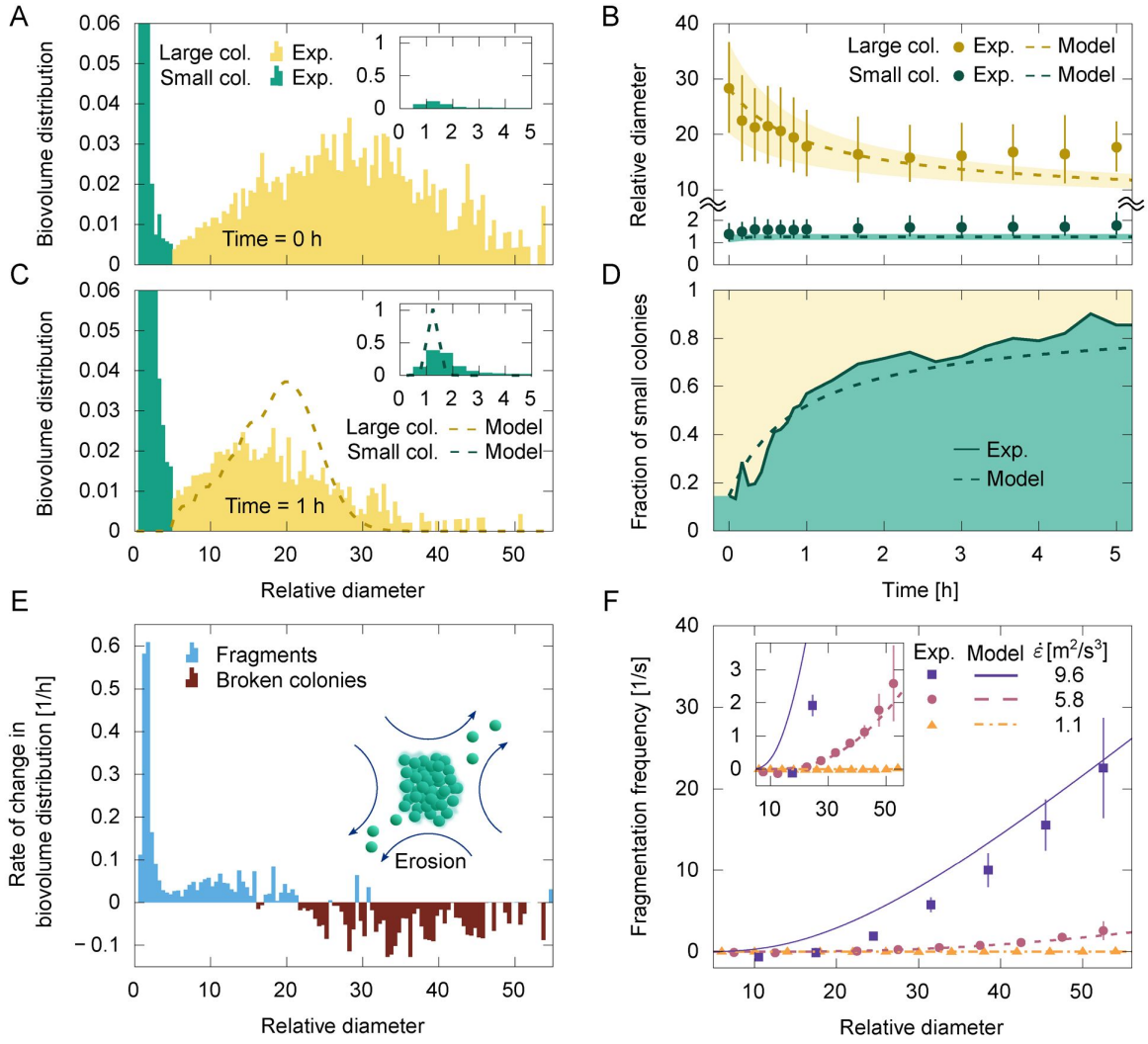

Fig. 2

Kinetics of fragmentation of *Microcystis* strain V163 colonies under cone-and-plate shear flow. The laboratory culture was filtered to select mainly large colonies, and the total biovolume fraction was adjusted to $\phi = 10^{-4}$. Suspensions were subjected to an intense dissipation rate ($\dot{\varepsilon} = 5.8\ m/s^3$) in panels A-E. (A) The initial size distribution of colonies, expressed as biovolume fraction of the relative colony diameter (normalized by single cell diameter). The size distribution had a bimodal shape, with large colonies (in yellow) and small colonies (in green, composed mostly of single cells, dimers, and some trimers, as depicted by the inset). (B) Median diameter of small and large colonies as a function of time. Bars indicate limits of 25th and 75th percentiles. (C) Most large colonies have been fragmented after 1 hour of shear flow, but the bimodal shape remained. (D) The size distribution shifted from large to small colonies as the shear flow induced fragmentation. (E) The rate of change in biovolume distribution at t = 0h. Negative values indicate loss of colonies by fragmentation, while positive values indicate newly created fragments. The distribution suggests an erosion mechanism, as depicted by the cartoon inside the plot. (F) Fragmentation frequency as a function of the relative diameter of colonies for three values of dissipation rate. The inset shows details for the low dissipation rates. Error bars indicate the standard deviation. Dashed lines and shaded regions in panels B-D indicate predictions from the population model given by **Eq. (1)**, and the lines in panel F indicate the predictions by **Eq. (4)**. Best fit parameters: $\alpha_1 = 0.023$, $S_1 = 0.034$, $q_1 = 4.5$, $S_2 = 31$, $q_2 = 4.1$.

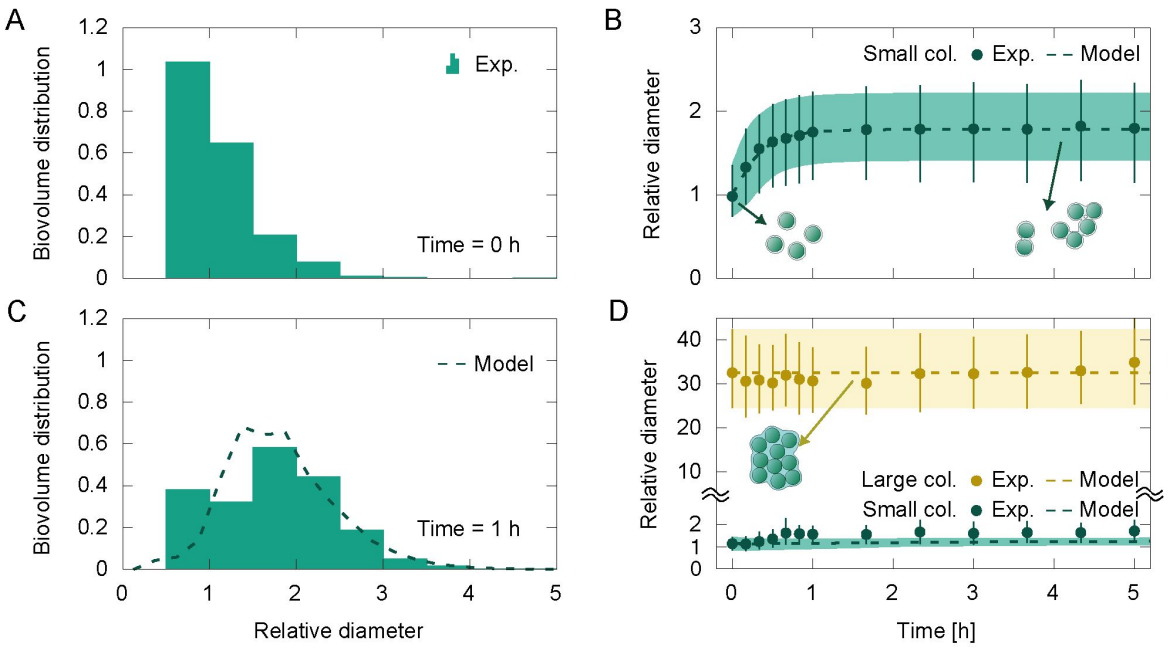

Fig. 3

Kinetics of aggregation for a single-cell suspension of *Microcystis* strain V163 at a moderate dissipation rate of $\dot{\varepsilon}$ = 0.019 m^2/s^3 and a total biovolume fraction of $\phi = 10^{-4}$. (A) Initial size distribution of the suspension as a function of the relative diameter, composed mostly of single cells. (B) Median diameter of colonies formed by aggregation of single cells as a function of time. Bars indicate limits of 25th and 75th percentiles. (C) After 1 hour of shear flow, the size distribution has shifted towards slightly larger diameters. (D) Time behavior of a suspension of large division-formed colonies under the same moderate dissipation rate and total biovolume fraction. The bimodal size distribution is separated into large (yellow) and small (green) colonies. Dashed lines and shaded regions in panels B-D indicate predictions from the population model given by **Eq. (1)**. Best fit parameters: $\alpha_1 = 0.023$, $S_1 = 0.034$, $q_1 = 4.5$, $S_2 = 31$, $q_2 = 4.1$.

where $l_o = (l^f - l'^f)^{1/f}$. The collision frequency is described by the kernel $\beta(l, l')$ and for a turbulent shear flow, we have $\beta(l,l') = 0.163(l+l')^3\sqrt{\dot{\varepsilon}/\nu}$, where ν is kinematic viscosity of the fluid [45]. The ratio of aggregative collisions over total collisions is given by the stickiness parameter α_i. For the category C_1 (aggregated colonies), the stickiness is positive, $\alpha_1 > 0$. In contrast, we neglect the aggregation of C_2 colonies (collisions between C_2–C_2 and C_1–C_2), since the bonds formed by aggregation would be weaker and quickly rupture again, such that $\alpha_2 = 0$. This assumption is corroborated by the absence of aggregation between large colonies in our experiments (**Fig. 3D**).

The colony formation will be limited by fragmentation if the colony exceeds a critical size $l_i^* = (\dot{\varepsilon}/S_i)^{-q_i/f}$, where S_i and q_i are constitutive parameters that depend on the aggregate structure and bond strength, with a lower bound at $l_i^* \geq 1$ [46, 47]. We assume that aggregation-formed colonies have a small critical size, as the overlap between the EPS layer of each cell is narrow, leading to weak bonds. Meanwhile, division-formed colonies have an EPS layer that fills the pores between cells, thus increasing the resistance to hydrodynamic stress. The fragmentation rate is given by a first-order kinetic equation [46]:

$$F_i(l,t) = -\kappa_i(l)\, n_i(l,t) + \int_l^\infty g_i(l,l')\, \kappa_i(l')\, n_i(l',t)\, \mathrm{d}l' \ , \tag{3}$$

where $\kappa_i(l)$ is the fragmentation frequency, which is a function of the probability distribution function of the hydrodynamic stress. Assuming a Gaussian distribution, the fragmentation frequency is [46]:

$$\kappa_i(l) = \sqrt{\frac{2\dot{\varepsilon}}{15\pi\nu}}\frac{\exp(-M_i^2)}{\mathrm{erf}(M_i)} \ , \tag{4}$$

where $M_i = \sqrt{15/2}\,(l/l_i^*)^{-f/2q_i}$. Due to the scarcity of experimental data in the literature, simplified models are usually assumed for the fragment distribution function $g_i(l,l')$, such as erosion, equal fragments, or a uniform distribution [48]. Assuming a binary fragmentation (*i.e.*, two fragments per fragmentation event), the fragment size distribution can be written in the form $g_i(l,l') = \delta(l - l_a) + \delta(l - l_b)$, where l_a and l_b are the sizes of fragments. Based on the results from division-formed colonies under intense dissipation rate (**Fig. 2E**), an ideal erosion mechanism is adopted for category C_2 colonies, such that $g_2(l,l') = \delta(l-1) + \delta(l - \sqrt[f]{l'^f - 1})$. In contrast, the experimental results for the small colonies (**Fig. 3C**) show a wider size distribution of eroded fragments which can not be captured by an ideal erosion mechanism, so an equal fragments mechanism is adopted for category C_1 colonies, *i.e.*, $g_2(l,l') = 2\delta(l - l'/\sqrt[f]{2})$. The size distributions of C_1 and C_2 colonies are coupled through a transfer rate of biovolume $T_i(l, t)$. We propose that the cells eroded from C_2 colonies are transferred to category C_1, such that:

$$T_1(l,t) = -T_2(l,t) = \delta(l-1)\int_l^\infty \kappa_2(l')\, n_2(l',t)\, \mathrm{d}l' \ , \tag{5}$$

while the complementary fragments of C_2 colonies remain in that category.

We solved the balance **equation (1)** using a zero-order discrete population balance, or sectional method, in which the size distribution is described by uniformly sized bins where the size distribution is evaluated at a representative size centered on the bin [48, 49]. The simulations were initialized with the size distributions at $t = 0$ obtained in our experiments. The two pairs of parameters for critical size ($\{q_1,S_1\}$ and $\{q_2,S_2\}$) and the stickiness parameter (a_1) were used to fit the model to the experimental data (*Materials and Methods*).

For an initial suspension composed mainly of large colonies at an intense dissipation rate ($\dot{\varepsilon} = 5.8\ m^2/s^3$),), the model prediction of a decrease in the median size of C_2 colonies up to a steady-state diameter is in good agreement with the experimental findings (**Fig. 2B**). Moreover, the erosion mechanism accurately predicts the biovolume transfer from C_2 to C_1 colonies (**Fig. 2D**). The use of the erosion mechanism for the fragment distribution function is further corroborated by previous studies simulating bacterial aggregates [50]. For C_1 colonies at this intense dissipation rate, the model predicts that their median diameter remains near $l^* = 1$ (*i.e.*, the lower bound for the critical size). However, the experimental results show a slightly wider size distribution of both the small and large colonies than predicted by an ideal erosion mechanism (**Fig. 2C**). Nevertheless, the global behavior of the size distribution is well described by the two-category model. Furthermore, a very good agreement is also observed between the measured fragmentation frequency and the mo del predictions given by **Eq.(4)** (**Fig. 2F**).

To complement the mathematical model and to further investigate the mechanical origins of the resistance of division-formed colonies to intense shear, we performed rheology tests on the cyanobacterial colonies (*Materials and Methods*). Simple and oscillatory shear measurements revealed elasto-viscoplastic mechanics [51, 52] of the concentrated aggregate with a yield stress of $\tau_y = 4.3 \pm 0.3$ Pa. The low volume fraction of cells in aggregate (~ 12 %) indicates that the mechanical properties are mainly dictated by the EPS layer. Equating the average hydrodynamic shear stress to the yield stress results in a critical colony size of $l_2^* = 2.8$ (Eq. 10 in *Materials and Methods*). The eroded fragments observed in the fragmentation experiments (**Fig. 2E**) are mostly smaller than this critical size. This suggests that large colonies will suffer erosion when the local hydrodynamic stress exceeds the yield stress of the EPS layer. Although the fracture behavior of colonies in suspension is expected to be different from a concentrated aggregate under shear rheology, the latter provides a reasonable and convenient estimate of the material properties of the colonies. Related to the critical size of the colony and their mechanical properties is the exponent q_2 (see **equation 4**). The best fit of the results in **Fig. 2** provided $q_2 = 4.1$. This value lies in the upper limit of previous results for colloidal aggregates [42, 46]. Note that for colloids, q is related to the stress concentration around cracks in the fractal structure of the aggregate [47], and low values of q are associated with brittle deformation, in which the stress concentration grows quickly with aggregate size. In contrast, cyanobacterial colonies have a soft plastic behavior that is less sensitive to large cracks, thus justifying the large value of q.

We further tested the model with the aggregation experiments. A suspension of C_1 colonies with an initial distribution close to the single-cell size (**Fig. 3A**) was simulated. The model agrees well with the experimental results for the median colony size, accurately predicting a steady-state value when there is a balance between collisions and fragmentation (**Fig. 3B**). The best fit of the results provided a small value for the stickiness parameter ($\alpha_1 = 0.023$). The aggregation rate is linearly dependent on the stickiness and the total biovolume fraction (**Eq. 2**), thus an increase in these parameters (α_1 and φ) allows the suspension to reach the steady-state size faster. However, the steady-state size has low sensitivity to these parameters (α_1 and φ), as the fragmentation frequency has a higher-order dependence with colony size (**Fig. 2F**). The equal fragments hypothesis leads to a single-peaked size distribution, whose steady-state median increases with the total biovolume fraction. If an ideal erosion mechanism was assumed for the C_1 colonies, the peak would be fixed around the single-cell size (*SI Appendix*, **Fig. S6**). The experimental results for the C_1 colonies are in better agreement with the equal fragments hypothesis (**Fig. 3C**).

Note that the ideal erosion and equal fragments mechanisms are idealized scenarios, and the real distribution is expected to be more dispersed. Furthermore, a fractal description of small colonies is limited, as a continuum function between biovolume and diameter of colonies may not hold. Moreover, the turbulent model used for fragmentation (**Eq. 4**) poses two limitations: (i) the theory was developed for homogeneous Gaussian turbulence [46], which differs considerably from the boundary-layer turbulence generated in a cone-and-plate shear [53], and (ii) the colonies were larger than the Kolmogorov scale for the intense dissipation rate used in our

fragmentation measurements (η = 20 μm for a dissipation rate of $\dot{\varepsilon} = 5.8\ m/s^3$, *SI Appendix*), meaning that the colony size is comparable to the smallest eddies in the flow. Despite these limitations, the proposed two-category model provides a good approximation of the fragmentation process observed in our experiments. Simulations that take into account spatially inhomogeneous and non-Gaussian turbulence are demanding and lack an explicit analytic expression for $\kappa(l)$ that can be applied to a population model [54].

Field Samples of *Microcystis* are more Resistant to Fragmentation due to Thicker EPS Layer

Samples of *Microcystis* spp. were collected from Lake Gaasperplas - the Netherlands (*Materials and Methods*). A major difference in fragmentation behavior is observed between the laboratory cultures of *Microcystis* strain V163 and the field samples of *Microcystis* spp. While the laboratory cultures suffered intense fragmentation at a dissipation rate of $\dot{\varepsilon} = 5.8\ m^2/s^3$, the colonies collected from the field showed negligible fragmentation at this dissipation rate (**Fig. 4A**). The size distribution of field colonies also had a bimodal shape both initially and after 1 hour of flow (**Figures 4C and E**). The small colonies displayed an increase in size due to aggregation up to 2.5x times the initial median size (**Fig. 4D**), although the fraction of small colonies remained below 11% even after a few hours of shear (**Fig. 4F**). The large colonies displayed only a small increase in size due to aggregation and quickly reached a steady-state size.

The higher resistance of field colonies to shear can be attributed to the thick EPS layer that surrounds the colony, which could be seen under brightfield microscopy using a negative staining (**Fig. 4B**, *Materials and Methods*). In contrast, this layer was barely visible in colonies of laboratory cultures of *Microcystis* strain V163. Nevertheless, the limited amount of aggregation observed for large field colonies indicates that aggregation-formed colonies have a smaller resistance to shear than division-formed colonies, similar to the results observed for laboratory colonies (**Fig. 3**). Differences in the morphology of colonies from field samples and laboratory cultures are frequently observed in the literature, with the latter often presenting only single cells or small colonies [55]. Colony formation may be influenced by various factors [17], where especially high calcium and low nitrogen concentrations are identified as factors promoting high EPS production [56–58]. This is consistent with the calcium and nitrogen concentrations measured in Lake Gaasperplas (71 mg/L Ca^{2+} and 0.04 mg/L N) *versus* BG-11 medium (9.8 mg/L Ca^{2+} and 246 mg/L N) (*Materials and Methods*).

Aggregation, Fragmentation, or Cell Division? A Guideline

Under which conditions are aggregation, fragmentation or cell division the dominant processes in colony formation? In a quiescent fluid, cyanobacterial colonies are expected to grow solely due to cell division with a specific growth rate $\mu = N_c^{-1}\mathrm{d}N_c/\mathrm{d}t$, which is a function of various environmental factors such as light intensity and nutrient availability [17, 20]. Let $\bar{l} = \int_0^\infty l\, n(l,t)\mathrm{d}l$ be the average colony size of a suspension. Assuming that the cells remain attached after division, the rate of increase in the average colony size will be

$$\frac{1}{\bar{l}}\frac{\mathrm{d}\bar{l}}{\mathrm{d}t} = \frac{\mu}{f}\ . \tag{6}$$

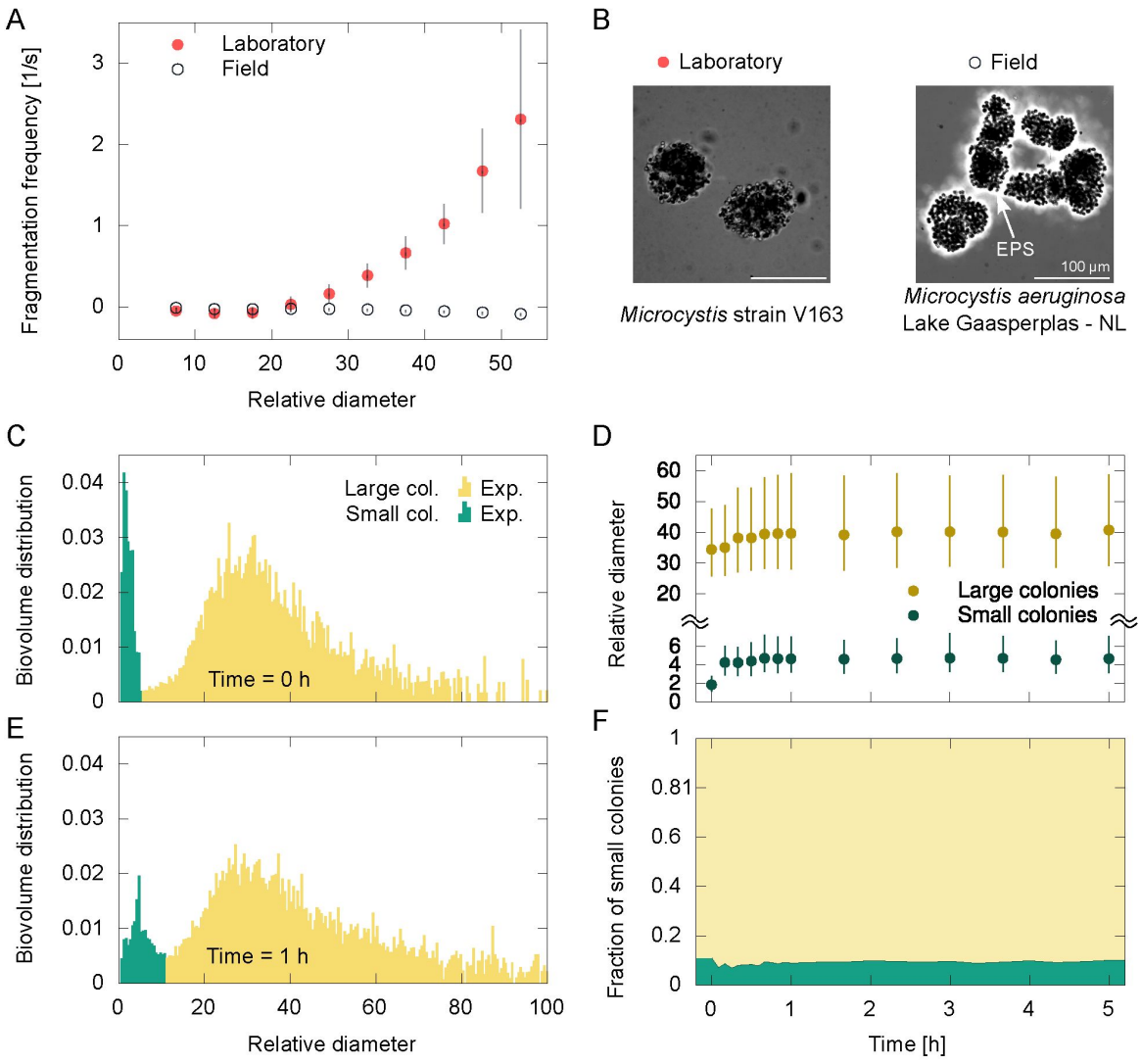

Fig. 4

Kinetics of the fragmentation of colonies in field samples of *Microcystis* spp. at an intense dissipation rate ($\dot{\varepsilon} = 5.8\ m^2/s^3$) and total biovolume fraction of $\phi = 10^{-4}$. (A) Comparison of the fragmentation frequency as a function of colony size for the laboratory culture (*Microcystis* strain V163) and the field samples (*Microcystis* spp.). Error bars indicate the standard deviation. (B) Brightfield microscopy images of colonies in a Nigrosin-dyed medium (dark region) show evidence of a thick EPS layer (bright region) surrounding a field colony. (C) Initial size distribution of colonies in field samples as a function of the relative diameter. The size distribution had a bimodal shape, with small colonies (green) and large colonies (yellow). (D) The median diameter of the colonies in each subpopulation as a function of time. Bars indicate 25th and 75th percentiles. (E) After 1 hour of shear flow, the small colonies have aggregated slightly, while the large colonies keept their size distribution. (F) The fraction of small colonies remained nearly constant during the experiment.

The increase in colony size will progress until a maximum size l_m is reached. The upper limit in colony size is still a subject of intense discussion, with species variability, reduced division rate at large sizes, and dissolution of the EPS layer being important factors [17, 31]. If the suspension is concentrated enough, collisions between colonies will also increase the average colony size due to aggregation. Let us consider initially a monodisperse suspension with a single size $\bar{l}$. At short times, the rate of increase in the average colony size due to aggregation will be (*SI Appendix*)

$$\frac{1}{\bar{l}}\frac{\mathrm{d}\bar{l}}{\mathrm{d}t} = 2.49(\sqrt[f]{2}-1)\,\phi\,\alpha\,\bar{l}^{\,4-2f}\sqrt{\frac{\dot{\varepsilon}}{\nu}}\,. \tag{7}$$

Assuming $f = 2$ for simplicity (which is similar to the measured value for *Microcystis* strain V163), we can use Eqs. (6) and (7) to define a dimensionless number *Ag*, quantifying the ratio between the rates of increase in the average colony size due to aggregation and cell division, given by

$$Ag = 2.06\,\frac{\alpha\,\phi}{\mu}\sqrt{\frac{\dot{\varepsilon}}{\nu}} \tag{8}$$

The dimensionless ratio A_g reveals the dominant mechanism for colony formation (cell division is dominant for $A_g \ll 1$, while aggregation is dominant for $A_g \gg 1$) and depends on the total biovolume fraction φ and dissipation rate $\dot{\varepsilon}$, as shown by the phase diagram in **Figure 5**. For a lake with a total biovolume fraction corresponding to an early bloom ($\varphi = 3 \cdot 10^{-7}$, according to WHO alert level 1 [59]), a low dissipation rate typical of wind-induced turbulence ($\dot{\varepsilon} \sim 10^{-7}\ m^2/s^3$) [60], a specific growth rate of $\mu \sim 0.008\ \mathrm{h}^{-1}$ [20], a kinematic viscosity of $\nu = 10^{-6}\mathrm{m}^2\mathrm{s}^{-1}$ and a stickiness of $\alpha \sim 0.02$, we estimate a ratio $A_g \sim 10^{-3}$. Under these conditions, the colony size increases due to cell division while the role of aggregation is negligible (region I in **Fig. 5**). In contrast, during a dense bloom event, the scum layer can reach a very high biovolume fraction of $\varphi \sim 10^{-2}$ [61, 62], which leads to $A_g \sim 10_2$ (keeping all remaining parameters constant). Therefore, colony formation in dense scum layers is dominated by colony aggregation (region II in **Fig. 5**). The aggregation process can form larger colonies which will have an enhanced buoyancy, thus assisting in the persistence of the scum layer.

Fragmentation limits the maximum colony size to a critical value *l**. Our experimental results (**Fig. 5**) indicate that aggregated colonies have a lower critical size than division-formed colonies for the same turbulence intensity. Conversely, a higher critical dissipation rate is needed for division-formed colonies ($\dot{\varepsilon}_{div}$) than for aggregated colonies ($\dot{\varepsilon}_{agg}$) to achieve the same critical size $l^* = l_m$. This creates an interesting regime at high biovolume fractions and dissipation rates in the range $\dot{\varepsilon}_{agg} < \dot{\varepsilon} < \dot{\varepsilon}_{div}$, in which only division-formed colonies can survive the turbulent flow, even though aggregation is faster than division ($A_g \gg 1$) (region III in **Fig. 5**). Typical values of critical dissipation rate for our experiments are $\dot{\varepsilon}_{agg} = 2.1 \cdot 10^{-3}\ m^2/s^3$ and $\dot{\varepsilon}_{div} = 3.7\ m^2/s^3$, assuming a maximum colony size of $l_m = 50$. Under natural turbulent conditions (*e.g.* surface wind-mixing), the dissipation rate is normally below $\dot{\varepsilon} \sim 10^{-6}\ m/s^3$ [60], which is insufficient to induce colony fragmentation. Artificial mixing systems can achieve levels of turbulence that are many orders of magnitude higher. In the core of bubble plumes, dissipation rates of $\dot{\varepsilon} \sim 10^{-4} - 10^{-1}\ m^2/s^3$ are reached [40]. This value was sufficient to prevent aggregation of large colonies in our experiments but was not high enough to induce fragmentation of division-formed colonies. Moreover, colonies remain only a short time (~ 1 min) in the bubble plume core, after which they are dispersed to weaker turbulent regions (dissipation rates of $\dot{\varepsilon} \sim 10^{-7} - 10^{-4}\ m^2/s^3$ just a few meters away from the bubble plume core). The intense hydrodynamic stress required to fragment division-formed colonies (region IV in **Fig. 5**) can only be achieved by mixers with fast-moving surfaces, such as the cone-and-plate setup used in our experiments ($\dot{\varepsilon} \sim 10^{-2} - 10^{1}\ m^2/s^3$) or

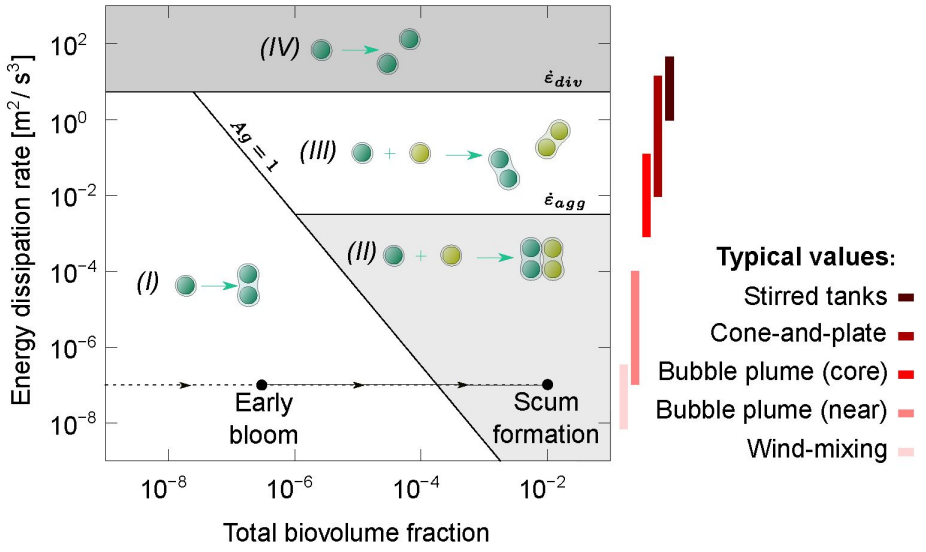

Fig. 5

Phase diagram indicating the dominant colony formation mechanism as a function of the dissipation rate $\dot{\epsilon}$ and the cyanobacterial abundance (expressed by the total biovolume fraction ϕ). (I) Colonies grow only by cell division at low dissipation rates and total biovolume fractions. (II) As the biovolume fraction increases, aggregation enhances colony growth. (III) For moderate dissipation rates, aggregated colonies are fragmented, and only cell division can increase colony size. (IV) Fragmentation of colonies dominates at intense dissipation rates, irrespective of whether these colonies were formed by aggregation or cell division. Bars on the right side indicate typical values of dissipation rate. The horizontal arrowed line indicates the transition from the absence of a bloom to a dense scum formation under typical wind mixing, with the bullets indicating the total biovolume fraction for WHO alert level 1 [59] (left) and for a typical scum layer [61] (right).

propellers used in stirred tanks ($\dot{\varepsilon} \sim 10^0 - 10^2\ m^2/s^3$) [41, 63]. These mixing devices can provide intense dissipation rates in small fluid volumes, but their implementation across entire lakes would be excessively energy-consuming.

Conclusions

Despite the widespread presence of bacterial colonies across species and environmental habitats, the influence of fluid flows on colony formation remains a fertile ground for continued exploration. A significant challenge is the lack of a generic framework in which the aggregation and fragmentation of colonies can be studied under various hydrodynamic stresses. We take a major step towards overcoming this challenge by presenting a combination of experiments and theory to elucidate the underlying mechanisms that determine the size distribution of cyanobacterial colonies over a wide range of flow intensities. Our experiments show that division-formed *Microcystis* colonies can be fragmented under intense dissipation rates $\dot{\varepsilon} \sim 3 - 10\ m^2/s^3$, following an erosion mechanism. Previous studies [32, 39] have observed significant fragmentation of *Microcystis* colonies in field samples at dissipation rates as low as $\dot{\varepsilon} \sim 10^{-4}\ m^2/s^3$. However, such studies primarily report volume averages of the dissipation rate, overlooking the likelihood of fragmentation occurring near fast-moving solid surfaces (grid stirrer [39] and propeller [32]), where the local hydrodynamic stresses are orders of magnitude higher. Instead, our results indicate that fragmentation of division-formed colonies can not be achieved with wind mixing or aeration systems.

We have demonstrated that flow-induced aggregated colonies of *Microcystis* form weaker structures than division-formed colonies, likely due to the weak EPS bonds between cells. Furthermore, we showed that colony aggregation is unlikely in lakes under early bloom conditions, as the collision frequency of colonies is too low. Our results, based on the mechanical properties of colonies, are corroborated by previous studies based on the sequencing of individual *Microcystis* colonies [25, 64]. These studies have identified that the genetic diversity within *Microcystis* colonies is much smaller than the diversity between *Microcystis* colonies, thus supporting the hypothesis that colony formation is dominated by cell division rather than by aggregation of colonies. Nonetheless, our results demonstrate that during scum formation in very dense blooms or phytoplankton patches, flow-induced aggregation likely plays a role and may quickly increase colony size. A summary of these outcomes is presented in the phase map illustrated in **Figure 5**.

From a broader perspective, our findings have relevance beyond predicting and mitigating cyanobacterial blooms. Since fluid flow affects the colonies and aggregates of many species [6–8, 65–67], the experimental methods and theoretical framework presented here, along with the identified mechanisms, could serve as a foundation to better understand the relationship between mechanics and biological functions and traits of colonies under hydrodynamic stresses and their morphodynamics and lifestyle. Other examples include non-natural settings, such as algae or cyanobacteria cultured in bioreactors, where dense cell populations experience intense mixing [68–70]. The results presented here could serve as design guidelines for such applications.

Materials and Methods

A. Sample preparation

Microcystis strain V163 cultured under laboratory conditions, as well as samples collected at Lake Gaasperplas - The Netherlands containing *Microcystis* spp. colonies were used for the experiments (**Fig. 1**). *Microcystis* strain V163 was originally isolated from Lake Volkerak - The Netherlands [71], grows in colonies and was obtained from the algal collection of the Institute for Biodiversity and Ecosystem Dynamics, University of Amsterdam. The *Microcystis* strain V163 was batch-cultured in Erlenmeyer flasks with standard BG-11 medium. The cultures were kept in an incubation chamber at a temperature of 20 °C. The light intensity was kept at 12 μmol photon $m^{-2}s^{-1}$ with a light:dark cycle of 14h:10h. The cultures were diluted with new BG-11 medium every week and kept at a maximum total biovolume fraction of $\varphi = 5 \cdot 10^{-4}$. The cultures were not shaken except after the addition of medium and before filtration. The *Microcystis* strain V163 has a single-cell diameter of $d_1 = 6.8 \pm 1.4$ μm (SD, N = 189). We categorize partially divided cells also as single cells, as these also behave as single units in a fragmentation/aggregation process. When considering only spherical cells not undergoing division, a diameter of 5.1 ± 0.8 μm (SD, N = 328) was obtained. Colonies of up to 500 μm were present in the culture under the incubation conditions as described before.

Samples of *Microcystis* spp. were collected from Lake Gaasperplas - the Netherlands (*SI Appendix* for water monitoring data and location of sampling point) on 14th August 2022. Water from the surface layer was filtered over a plankton net with a 100 μm mesh size. Samples were kept refrigerated at 4 °C, and the experiments were conducted over the next three days. The plankton composition was dominated by *Microcystis* spp. (89 ± 7% , SD, $N = 231$), with *Microcystis aeruginosa* being the main morphospecies, with an average single-cell diameter of $d_1 = 7.0 \pm 1.4$ μm (SD, $N = 100$). Colonies of *Dolichospermum spp.* were present in lower numbers. However, no differentiation of colony species was made during image processing, as it was not feasible to isolate them.

Negative staining was used to verify for the presence of an EPS layer surrounding the colonies of *Microcystis* strain V163 and of *Microcystis* spp. in field samples. Nigrosin was added to the surrounding medium, causing the EPS layer to appear bright under brightfield microscopy.

Upon appropriate filtering of the culture, we obtained a suspension with a specific size range. Filter paper with a 25 μm pore size was used to obtain a suspension primarily consisting of single cells (colonies with 2 or 3 cells also present in small numbers). For a suspension mainly comprising large colonies, we filtered the culture with 53 μm nylon mesh. The colonies collected in the mesh were then redispersed in a new BG-11 medium. To estimate the total biovolume fraction of the suspension, 1 ml of the sample underwent a heat treatment to disaggregate colonies [72]. At least 1000 cells were counted in a Neubauer hemocytometer assisted by the image processing software *ImageJ*. The total biovolume fraction of the suspension was calculated as $\varphi = cv_1$, where c is the cell concentration and v_1 is the average single-cell volume. Prior to each experiment, the desired biovolume fraction was adjusted using new BG-11 medium for the *Microcystis* strain V163 culture and with filtered (0.8μm) water from Lake Gaasperplas for field samples of *Microcystis* spp..

B. Cone-and-plate shear

A cone-and-plate shear flow was selected for our experiments (**Fig. 1B** and SI). This geometry is commonly used for standard rheological measurements because it provides a homogeneous shear rate under a laminar flow regime. Although less common in inertial regimes, it has been recommended by previous studies to investigate the effects of hydrodynamic stress in tissues [53, 73, 74]. Furthermore, the mixing provided by turbulence helps maintain a homogeneous concentration throughout the suspension.

Our setup consists of an upper conical probe made from transparent acrylic, with an outer diameter of 42 mm and a cone complementary angle of θ = 5.44° (Fig. SI). The conical probe is attached to a steel shaft, and it is driven by a rheometer head Anton Paar DSR 502. The lower surface consists of a 1mm thick glass slide. A cylindrical acrylic ring confines the fluid, preventing spillage of the sample due to strong centrifugal forces. The inner diameter of the ring is 46 mm, which ensures that the nominal shear rate between the upper probe's outer surface and the ring is the same as between the conical and lower surfaces. A clearance gap of 10 μm was set between the tip of the cone and the lower surface to avoid solid-solid friction.

At low rotational speeds, the flow is laminar with a homogeneous shear rate $\dot{\gamma}_n = \omega/\theta$, where ω is the angular velocity of the conical probe. The flow transitions to a turbulent regime at faster rotations, as the inertial forces become dominant. Since the shear rate is not uniform at the non-linear regime, the nominal shear rate $\dot{\gamma}_n$ is no longer an appropriate measure for shear intensity. Instead, the average intensity is given by the energy dissipation rate $\dot{\varepsilon}$, which measures the rate of energy loss by viscous dissipation per unit fluid mass. Under steady-state conditions, this dissipation rate balances the power injected into the fluid, therefore:

$$\dot{\varepsilon} = \frac{T\,\omega}{\rho\,V}\ , \tag{9}$$

where ρ and V are, respectively, the density and volume of the fluid sample, and T is the torque on the conical probe, measured by the rheometer head. The flow regime can be identified from the energy dissipation rate curve against the angular velocity, with a ~ ω^2 dependence in the laminar regime and a ~ $\omega^{5/2}$ dependence in the turbulent regime (*SI Appendix*, **Fig. S7B**). All shear experiments conducted in this work were in the latter regime. The average hydrodynamic shear stress can be calculated from the dissipation rate by

$$\overline{\tau}_t = \rho\sqrt{\nu\,\dot{\varepsilon}}. \tag{10}$$

The experimental setup provides a configuration where the dissipation rate can be controlled over a large range, while stress values can be measured with high precision. This, combined with optical access and simultaneous microscopy, presents a well-suited tool to study the response of biological samples under fluid flow.

C. Fragmentation and aggregation experiments

The fragmentation and aggregation experiments involved subjecting a suspension of *Microcystis* colonies to the cone-and-plate shear and using brightfield microscopy to image the colonies under shear. The lower surface was positioned on top of an inverted microscope Nikon TS100 with a 4x objective lens. The center of the field of view was located 15 *mm* from the rotation axis and with the focal plane set 0.5 *mm* above the lower surface. Illumination was provided by a Schott KL 1500 HAL light source equipped with a cyan filter (low pass with a cut-off wavelength of 555 *nm*) to minimize the photosynthetic activity of the sample. Images were captured with a Prime BSI Express sCMOS camera with a resolution of 1.63 *μm* per pixel. Prior to each experiment, a reference background image was created using distilled water, which was then discarded. A volume of 3.5 *ml* of the suspension of *Microcystis* colonies was pipetted in between the shear surfaces. The shear protocol was as follows: pre-shear at $\dot{\varepsilon} = 1.1\ m^2/s^3$ for 1 minute to mix the suspension; 12 shear cycles of 5 minutes each followed by 12 cycles of 20 minutes each at the target dissipation rate (imaging cycles, at low dissipation rate of 0.019 m^2/s^3 for 1 min, were intercalated with each shear cycle). During the imaging cycles, 200 frames were captured at a rate of 10 *fps*, ensuring that each frame was sampled over a different set of colonies. Examples of the captured frames are shown in **Figure 1**.

D. Image analysis

The frames underwent pre-processing with background subtraction and thresholding (*SI Appendix*). Image segmentation was performed with the *Scikit Image* library for Python [75]. Colony size was determined by their Feret diameter d, which represents the maximum distance between two boundary points of the colony. The number of cells in a colony was estimated from the diameter using the formula $N_c = (d/d_1)^f$, where f is the average fractal dimension of the colonies. Since not all colonies were within the depth-of-focus, a correction function for the colony count was estimated using a suspension with a known size distribution. The image magnification was optimized for intermediate and large colonies Given the wide range of colonies (from single cells ≈ 7μm to large colonies ≈ 500μm). Colonies smaller than 25μm were measured with lower precision, necessitating a second correction function for accurate counting (*SI Appendix*, Eq. S1).

To estimate the colony fractal dimension f, a reference sample of colonies had its size distribution characterized in a cylindrical counting chamber, followed by measurement of the total cell count in a hemocytometer. The fractal dimension was fitted such that the estimated cell count was equal to the measured count. For *Microcystis* strain V163, a value of $f = 2.09$ was obtained, while for the field samples of *Microcystis* spp. it was 1.64.

For the direct computation of the fragmentation frequency, we assume a pure fragmentation with an ideal binary erosion, such that the time derivative of the colony size distribution is

$$\frac{d}{dt}N_p[i](t) = -\frac{\kappa[i]\,N_p[i](t)}{l^f[i] - l^f[i-1]} + \frac{\kappa[i+1]\,N_p[i+1](t)}{l^f[i+1] - l^f[i]}\,, \tag{11}$$

where $N_p\,[i](t)$, $\kappa[i]$, and $l[i]$ refer to the bin count, fragmentation frequency, and relative diameter at the center of bin i. This formula is only valid for the bins larger than the single cell, as the latter does not suffer fragmentation. The bin count is initialized with the experimental value and evolved in time using an implicit Radau scheme (*SI Appendix*). The fragmentation frequency of K_b of each bin was obtained by minimizing the squared error between the experimental and numerical bin counts. The script for image analysis is available here. Detected features for all datasets and raw images for the dataset in **Fig. 2A-E** are available here.

E. Yield stress of cyanobacterial colonies

The mechanical resistance of *Microcystis* colonies can be estimated by separating the colonies from the medium and measuring the yield stress of the concentrated aggregate. A suspension of *Microcystis* strain V163 was filtered through a 53 μm mesh, and the large colonies were resuspended in fresh BG-11 medium. The sample was centrifuged for 30 min at 1000 g, and the pellet was separated. A dense gelatinous phase composed of cells and EPS was obtained, with cells accounting for 12% of the total biovolume fraction. The yield stress of the concentrated aggregate was measured with an Anton Paar MCR 301 rheometer. The upper probe was a sand-blasted 50 mm cone with 1 ° angle, while the lower surface was covered with sandpaper to avoid wall slip. Each sample was pre-sheared at 10 s^{-1} for 2 minutes. Steady-shear and large amplitude oscillatory shear tests were performed (*SI Appendix*, **Fig. S5**). From a Herschel-Bulkley fit over the steady shear data, $\tau = \tau_y + k\dot{\gamma}^n$, the dynamical yield stress $\tau_y = 4.3 \pm 0.3$ Pa (SD from best fit) was estimated. Due to the limited volume of samples available, only one repetition was possible for steady shear and oscillatory shear tests each.

F. Simulations

The balance **equation (1)** for the total normalized biovolume distribution was solved numerically using a zeroorder discrete population balance, or sectional method, in which the size distribution is described by uniformly sized bins, and the biovolume distribution is evaluated at a

representative size centered on the bin[48]. The integrals for the aggregation (Eq. 2), fragmentation (Eq. 3), and transfer (Eq. 5) rates were discretized with the approach by [49]. The biovolume distribution evolved in time with a Runge-Kutta 4-5 adaptive time step scheme written in Fortran. The simulation results were fitted with the experimental data by minimizing the absolute error of each category's 25th, 50th, and 75th percentiles of the biovolume distribution, using a Nelder-Mead algorithm [76]. The stickiness α_1 and for the pair of constitutive parameters S_1 and q_1 for the critical size of small colonies (category C_1) were obtained by fitting the model to the dataset of a single-cell suspension under $\dot{\varepsilon} = 0.019\ m^2/s^3$ and φ = 0.01. The pair of constitutive parameters S_2 and q_2 for the critical size of large colonies (category C_2) were obtained by fitting the model to the dataset of a large colony suspension under $\dot{\varepsilon} = 0.019\ m^2/s^3$ = 5.8 m^2/s^3 and φ = 0.01. These datasets were chosen as their aggregation/fragmentation times were similar to the measurement time, while for the other datasets, the variations were either too fast or slow to be captured in detail. The script for the simulation is available here.

Supporting Information Text

Field sample collection

Samples of *Microcystis* spp. were collected from Lake Gaasperplas - the Netherlands - at the sampling point 52°18'31.0"N 4°59'59.2"E on 14th August 2022, at 14:00. This is an artificial lake used for recreational purposes. No visible surface scums were present at the time of sampling. Water quality measurements of Lake Gaasperplas were obtained from the Dutch Water Authority (Rijkswaterstaat). **Figure S1** shows micrographic images of the phytoplankton samples.

Image analysis

This section describes the routine used to analyze raw images of the aggregation and fragmentation process of *Microcystis* colonies under a cone-and-plate shear setup. Each frame has dimensions of 2048x2048 pixels. Prior to each experiment, 3.5 ml of distilled water was pipette in the setup, and 200 frames were captured at $\dot{\varepsilon}$ and 10 fps. A background image was generated by averaging over the frames and applying a Gaussian blur filter. After that, the distilled water was discarded, and 3.5 ml of cyanobacteria suspension was pipetted into the setup. Each time point in the data sets corresponds to a stack of 200 frames. Two treatments are made, one to detect small colonies(or single cells) and another to detect large colonies:

- Small colonies (l < 5): Image is cropped into a smaller section (500x500 pixels), to speed the processing. The background is subtracted using the reference image. The image intensity is renormalized and then thresholded. Small features (0.5 < l < 5) are segmented, measured, and counted.
- Large colonies (l > 5): A Gaussian blur is applied to filter small colonies. The background is subtracted using a reference image. The image intensity is renormalized and then thresholded. Small features (l > 5) are segmented, measured, and counted.

For each time point, the counted features of the 200 frames were distributed in bins of width Δl = 0.5. Since not all colonies are within the depth-of-focus, a correction function for the featured count was estimated using a suspension with a known size distribution, given by:

$$N_c[i] = \begin{cases} (\lambda_3 + \lambda_1 (\lambda_2 - \lambda_3))\, N_p[i] & , \text{ if } l[i] \leq 2 \\ (\lambda_3 + \lambda_1 (\lambda_2 - \lambda_3)(4 - l[i])/2)\, N_p[i] & , \text{ if } 2 < l[i] \leq 4 \\ \lambda_3\, N_p[i] & , \text{ if } 4 < l[i] \leq 5 \\ \lambda_4\, N_p[i] & , \text{ if } l[i] > 5 \end{cases} \quad \text{(S1)}$$

Here, N_p [i] and N_c [i] are the number of features before and after correction in a bin centered at l[i]. To obtain the calibration parameters λ_i, a sample of filtered colonies of *Microcystis* strain V163 was subjected to the cone-and-plate shear setup for 2 min at $\dot{\varepsilon} = 0.019\ m^2/s^3$, and then transferred to a counting chamber. The latter was used as a standard for the size distribution. The calculated parameters were $\lambda_1 = 1$, $\lambda_2 = 73.13$, $\lambda_3 = 13.71$ and $\lambda_4 = 1.24$. The small size range ($l \leq 4$) has low precision due to the pixel resolution, therefore the parameter λ_1 was adjusted to ensure biovolume conservation. The value of $\lambda = 1$ was used for $t = 0$, and it was fitted in each subsequent time point so that the total cell count is constant through time. Finally, the normalized biovolume distribution for each time point is calculated.

For the direct computation of the fragmentation frequency, a pure fragmentation with an ideal binary erosion was assumed, such that the time derivative of the colony size distribution is

$$\frac{\mathrm{d}}{\mathrm{d}t} N_p[i](t) = -\frac{\kappa[i]\, N_p[i](t)}{l^f[i] - l^f[i-1]} + \frac{\kappa[i+1]\, N_p[i+1](t)}{l^f[i+1] - l^f[i]}\ , \tag{S2}$$

where N_p [i](t), κ[i], and l[i] refer to the bin count, fragmentation frequency, and relative diameter at the center of bin i. This formula is only valid for the bins larger than the single cell, as the latter does not suffer fragmentation. The bin count distribution N_p [i] is initialized with the experimental value, and an initial guess fragmentation frequency κ[i] is made for all bins larger than a single cell. The values of N_p [i] are evolved in time using the Python solver scipy.integrate.solve_ivp, with an implicit Radau method. For each bin, the cumulative squared error between the experimental and numerical bin counts is computed. The error is minimized using the values of κ[i] as the optimization parameter and the Python solver scipy.optimize.minimize. The uncertainty of κ[i] is propagated from (S2) talking into account the bin count uncertainty. The bin size for each dataset was chosen in order to minimize the bin count uncertainty. The script for image analysis is available here.

Fragmentation measurements with *Microcystis* strain V163

Additional measurements of fragmentation of large colonies of *Microcystis* strain V163 were performed. Colonies grown by cell division were filtered through a mesh of 53 μm, and the collected colonies were redispersed in BG-11 medium. Under moderate dissipation rate of $\dot{\varepsilon} = 0.019\ m/s^3$ the fragmentation was negligible (**Fig. S2**), with the median size and fraction of large colonies remaining stable over 5 hours of flow. The behavior is independent of the total biovolume fraction, showing that aggregation rates are negligible for large colonies. In contrast, the steady median size for small colonies increases with the total biovolume fraction, although still an order of magnitude smaller than division-formed colonies. Significant fragmentation can be seen from a dissipation rate of $\dot{\varepsilon} = 5.8\ m/s^3$ (**Fig. S3**). For a large value of $\dot{\varepsilon} = 9.6\ m/s^3$, the small colonies become the largest fraction in below 5 min (the smallest time resolution in our setup).

Aggregation measurements with *Microcystis* strain V163

Additional measurements of aggregation of single cells of *Microcystis* strain V163 were performed. The suspension was filtered through a 25 μm filter paper to select mostly single cells. Under moderate dissipation rate of $\dot{\varepsilon} = 0.019\ m/s^3$, the aggregation increased with the total biovolume fraction φ (**Fig. S4**). Under an intense dissipation rate of $\dot{\varepsilon} = 5.8\ m/s^3$, no aggregation was observed, and the median size of colonies remained equal to the initial value (near the single-cell size).

Rate of increase in the average colony size due to pure aggregation

Consider a suspension of colonies subjected only to aggregation, neglecting cell division and fragmentation. In this case, the time derivative of the normalized biovolume distribution $n(l, t)$ is given by [1]:

$$\frac{\partial}{\partial t}n(l,t) = \frac{6\,\phi\,\alpha}{\pi}\left[\frac{1}{2}\int_0^{l}\beta(l',l_o)\left(\frac{l}{l'l_o}\right)^{2f-1} n(l',t)\,n(l_o,t)\,\mathrm{d}l' - n(l,t)\int_0^{\infty}\beta(l,l')\,\frac{1}{l'^{f}}\,n(l',t)\,\mathrm{d}l'\right], \tag{S3}$$

where $l_o = (l^f - l'^f)^{1/f}$, and the collision frequency kernel is $\beta(l,l')$. The average colony size is defined as $\bar{l} = \int_0^{\infty} l\,n(l,t)\mathrm{d}l$. Applying this definition to Eq. (S3), we obtain that the time derivate of $\bar{l}\,(t)$ follows:

$$\frac{\partial}{\partial t}\bar{l}(t) = \frac{6\,\phi\,\alpha}{\pi}\left[\frac{1}{2}\int_0^{\infty}\int_0^{l}\beta(l',l_o)\,l\left(\frac{l}{l'\,l_o}\right)^{2f-1} n(l',t)\,n(l_o,t)\,\mathrm{d}l'\mathrm{d}l - \int_0^{\infty}\int_0^{\infty} n(l,t)\,\beta(l,l')\,l\,\frac{1}{l'^{f}}n(l',t)\,\mathrm{d}l'\mathrm{d}l\right]. \tag{S4}$$

If we assume that the size distribution remains monodisperse for short times, we can write that $n(l, t) = \delta(l - \bar{l}\,(t))$. Substituting this hypothesis into Eq. (S4) results that

$$\frac{\partial}{\partial t}\bar{l}(t) = \frac{6\,\phi\,\alpha}{\pi}\left[\frac{1}{2}\int_0^{\infty}\int_0^{l}\beta(l',l_o)\,l\left(\frac{l}{l'l_o}\right)^{2f-1}\delta(l'-\bar{l})\,\delta(l_o-\bar{l})\,\mathrm{d}l'\mathrm{d}l - \int_0^{\infty}\int_0^{\infty}\delta(l-\bar{l})\,\beta(l,l')\,l\,\frac{1}{l'^{f}}\,\delta(l'-\bar{l})\,\mathrm{d}l'\mathrm{d}l\right]. \tag{S5}$$

Applying a variable change, the integral can be rewritten as:

$$\frac{\partial}{\partial t}\bar{l}(t) = \frac{6\,\phi\,\alpha}{\pi}\left[\frac{1}{2}\int_0^{\infty}\int_0^{\infty}\beta(l',l_o)\,l\left(\frac{l}{l'l_o}\right)^{2f-1}\delta(l'-\bar{l})\,\delta(l_o-\bar{l})\,l_o^{f-1}\,(l_o^f+l'^f)^{\frac{1}{f}-1}\,\mathrm{d}l_o\mathrm{d}l' - \int_0^{\infty}\int_0^{\infty}\delta(l-\bar{l})\,\beta(l,l')\,l\,\frac{1}{l'^{f}}\,\delta(l'-\bar{l})\,\mathrm{d}l'\mathrm{d}l\right]. \tag{S6}$$

Solving the integral and applying the model for the collision kernel in a turbulent shear flow [2], $\beta(l, l') = 0.163\,(l + l')^3\,\sqrt{\dot{\varepsilon}/\nu}$, results that the rate of increase in the average colony size is:

$$\frac{1}{\bar{l}}\frac{\mathrm{d}\bar{l}}{\mathrm{d}t} = 2.49\,(\sqrt[f]{2}-1)\,\phi\,\alpha\,\bar{l}^{\,4-2f}\sqrt{\frac{\dot{\varepsilon}}{\nu}}\,. \tag{S7}$$

In the limit of fractal dimension $f = 2$, the growth rate reduces to;

$$\frac{1}{\bar{l}}\frac{\mathrm{d}\bar{l}}{\mathrm{d}t} = 1.03\,\phi\,\alpha\,\sqrt{\frac{\dot{\varepsilon}}{\nu}}\,, \tag{S8}$$

which is independent of $\bar{l}$.

Rheological characterization of concentrated colonies of *Microcystis* strain V163

A steady-shear (**Fig. S5A**) and a large-amplitude-oscillatory-shear (**Fig. S5B**) tests were performed in a sample of concentrated colonies of *Microcystis* strain V163. Due to the limited volume of samples available after separation, only one repetition was possible for each test. Before each test, the sample was subject to a preshear at $\dot{\gamma} = 10\ \mathrm{s}^{-1}$ for 200s, followed by 100s of rest. For the steady-shear test, the minimum transient time was determined in a separate test (40s for $\dot{\gamma} = 100\ \mathrm{s}^{-1}$ to 200s for $\dot{\gamma} = 0.001\ \mathrm{s}^{-1}$). For the oscillatory shear, the minimum transient time was determined by the rheometer software. A Herschel-Bulkley fit was applied to the steady shear data, $\tau = \tau_y + k\dot{\gamma}^n$, from which a dynamical yield stress τ_y = 4.3 ± 0.3 Pa (SD from best fit) was estimated.

Comparison of hypothesis for the fragment distribution function

Assuming a binary fragmentation (*i.e.,* two fragments per fragmentation event), the fragment size distribution can be written in the form $g_i(l, l') = \delta(l - l_a) + \delta(l - l_b)$, where l_a and l_b are the size of fragments. Two ideal models for binary fragmentation are erosion and equal fragments, described by the following functions:

$$g(l, l') = \begin{cases} \delta(l-1) + \delta(l - \sqrt[f]{l'^f - 1}) & (\text{Erosion}), \\ 2\delta(l - l'/\sqrt[f]{2}) & (\text{Equal fragments}). \end{cases} \tag{S9}$$

Due to a lack of experimental evidence of single colony fragmentation events, both models were tested for the category C_2 colonies. The equal fragments hypothesis was chosen as it better captures the experimental results for the size distribution of *Microcystis* strain V163 colonies aggregated from single cells (**Fig. S6**).

Cone-and-plate shear setup

The turbulent shear was generated by a cone-and-plate shear, with the dimensions depicted in **Fig. S7A**. The flow regime can be identified from the average energy dissipation rate $\dot{\varepsilon}$ curve against the angular velocity ω, with a ~ ω^2 dependence in the laminar regime and a ~ $\omega^{5/2}$ dependence in the inertial region (**Fig. S7B**) [3, 4]. The Kolmogorov scale η, which is an estimate of the size of the smallest eddies in a turbulent flow, can be calculated from the relation $\eta = \nu^{3/4}\dot{\varepsilon}^{-1/4}$. The Kolmogorov scale in our results range from η ~ 85 μm for the lowest dissipation rate ($\dot{\varepsilon} = 0.019\ m^2/s^3$) to η ~ 18 μm for the highest dissipation rate ($\dot{\varepsilon} = 9.6\ m^2/s^3$).

Acknowledgements

We thank Maria van Herk, Pieter Slot, and Merijn Schuurmans for their support with laboratory cultures. We are grateful to Axel Gunderson for his assistance with fieldwork, and to Daan Giesen for his support with experimental setup design. We especially thank Johan Oosterbaan and Richard Steel for their contributions during the project's conception. We acknowledge funding from the Hoogheemraadschap van Rijnland. MJ acknowledges support from the ERC grant no. "2023-StG-101117025, FluMAB.

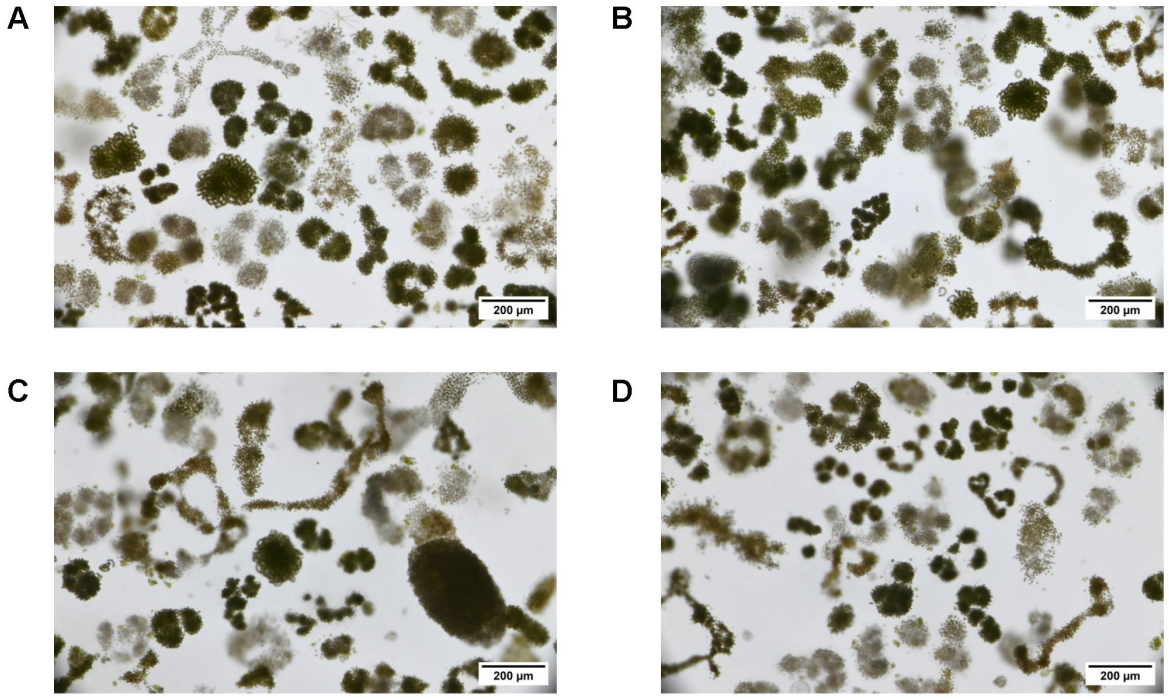

Fig. S1

(A-D) Micrographic images of phytoplankton field samples collected from the surface layer of Lake Gaasperplas. *Microcystis* spp. are dominant in the sample.

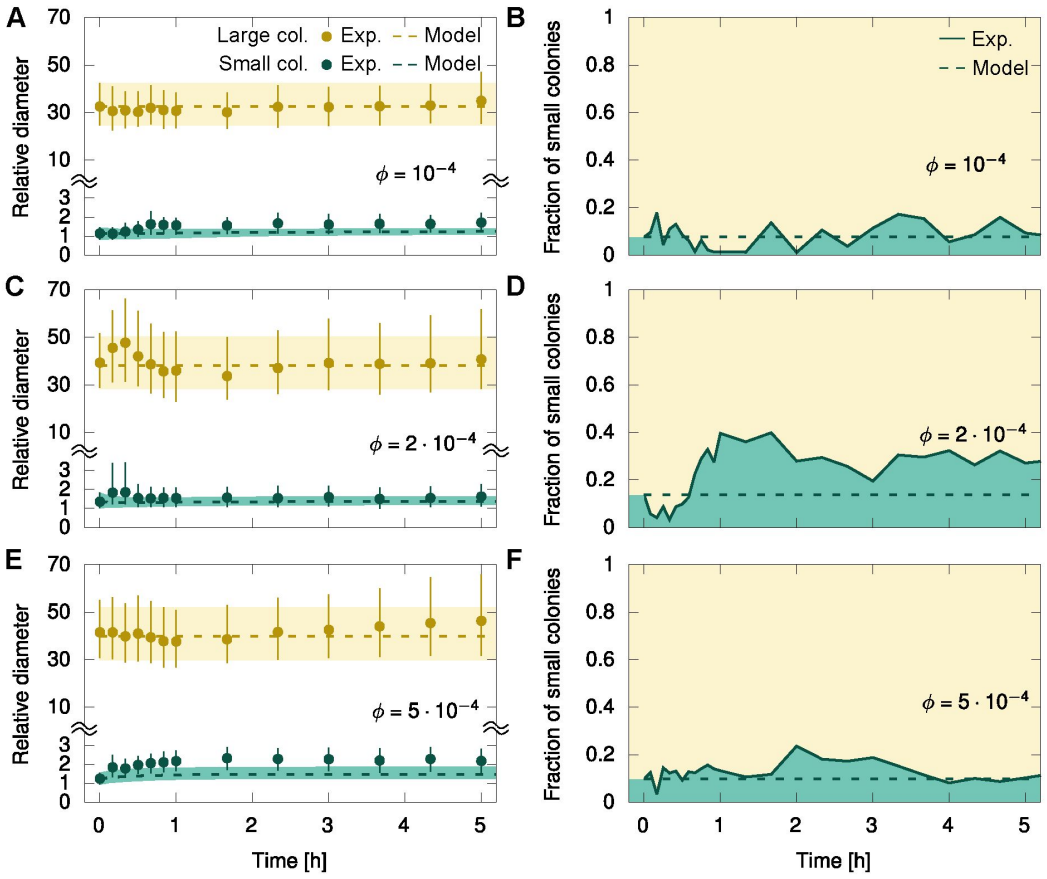

Fig. S2

Kinetics of the fragmentation of *Microcystis* strain V163 colonies under a moderate dissipation rate ($\dot{\varepsilon} = 0.019\ m/s^3$) and various values of total biovolume fraction. The laboratory culture was filtered to select mainly large colonies, and total biovolume fraction was adjusted. Plots in the left column depict the median diameter of each size population as a function of time, where bars and shaded regions indicate limits of 25th and 75th percentiles. Plots in the right column depict the fraction of small colonies as a function of time. The total biovolume fraction is (A-B) $\phi = 10^{-4}$, (C-D) $\phi = 2 \cdot 10^{-4}$, (E-D) $\phi = 5 \cdot 10^{-4}$. Best fit parameters: $\alpha_1 = 0.023$, $S_1 = 0.034$, $q_1 = 4.5$, $S_2 = 31$, $q_2 = 4.1$.

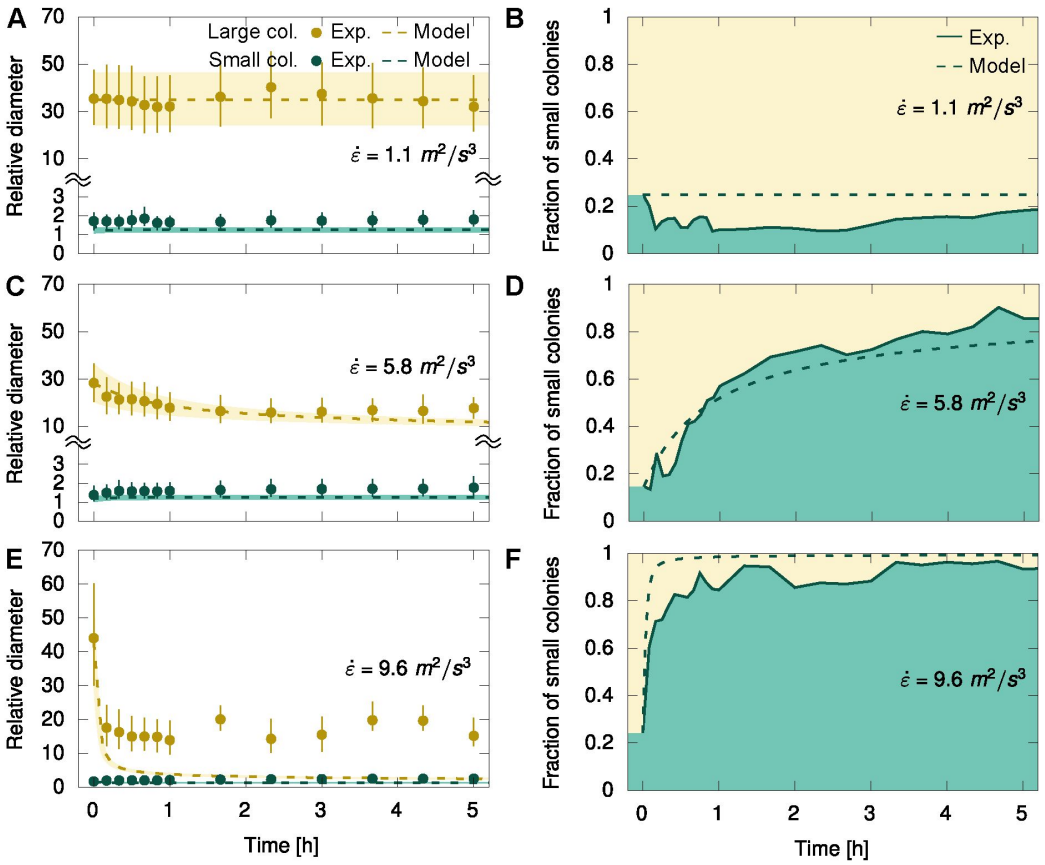

Fig. S3

Kinetics of the fragmentation of strain V163 colonies under a moderate total biovolume fraction (ϕ = 10_{-4}) and various values of dissipation rate. The laboratory culture was filtered to select mainly large colonies, and total biovolume fraction was adjusted. Plots in the left column depict the median diameter of each size population as a function of time, where bars and shaded regions indicate limits of 25th and 75th percentiles. Plots in the right column depict the fraction of small colonies as a function of time. The dissipation rate is (A-B) $\dot{\varepsilon} = 1.1\ m/s^3$, (C-D) $\dot{\varepsilon} = 5.8\ m/s^3$, (E-D) $\dot{\varepsilon} = 9.6\ m/s^3$. Best fit parameters: α_1 = 0.023, S_1 = 0.034 , q_1 = 4.5, S_2 = 31 , q_2 = 4.1.

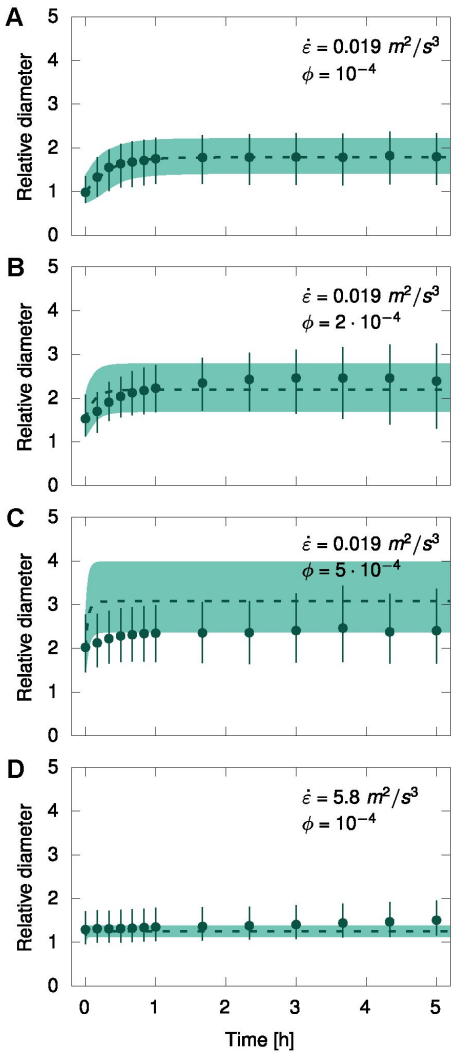

Fig. S4

Kinetics of the aggregation of *Microcystis* strain V163 colonies under a moderate dissipation rate ($\dot{\varepsilon} = 0.019\ m^2/s^3$) and various values of total biovolume fraction. The laboratory culture was filtered to select mostly single cells, and the total biovolume fraction was adjusted. Plots in the left column depict the median diameter of each size population as a function of time, where bars and shaded regions indicate limits of 25th and 75th percentiles. Plots in the right column depict the fraction of small colonies as a function of time. The total biovolume fraction is (A-B) $\phi = 10^{-4}$, (C-D) $\phi = 2 \cdot 10^{-4}$, (E-D) $\phi = 5 \cdot 10^{-4}$. Best fit parameters: $\alpha_1 = 0.023$, $S_1 = 0.034$, $q_1 = 4.5$, $S_2 = 31$, $q_2 = 4.1$.

Fig. S5

Rheology of concentrated colonies of *Microcystis* strain V163. (A) Shear stress as a function of the shear rate obtained for a steady shear test. Solid line indicates a Herschel–Bulkley fit, $\tau = \tau_y + k\dot{\gamma}^n$, where τ_y = 4.3 ± 0.3Pa (SD from best fit) is the dynamical yield stress. Other fit parameters are k = 0.55 ± 0.13 and n = 0.85 ± 0.05 (B) Storage G' and loss G'' moduli as a function of the deformation strain amplitude γ for a oscillatory shear with angular frequency of 1 rad/s.

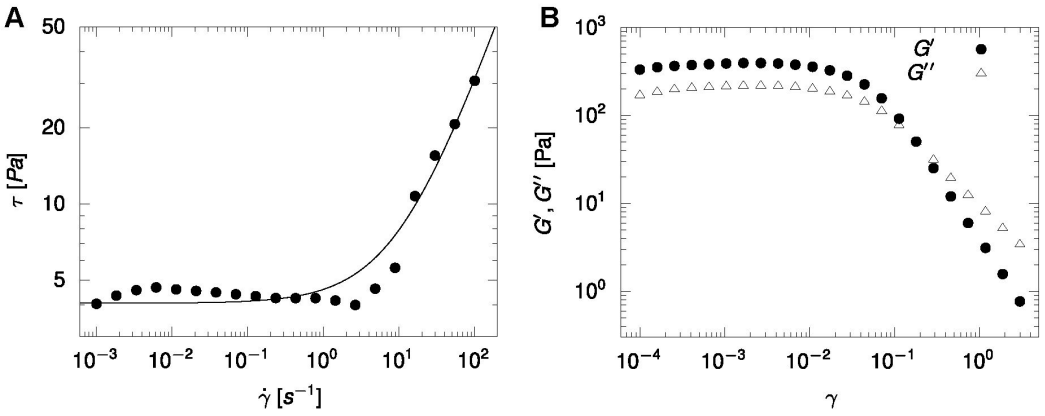

Fig. S6

Comparison of hypothesis for the fragment distribution of category C_1 colonies. Bars show the experimental results for normalized biovolume distribution of filtered single cells of *Microcystis* strain V163 after 1 hour under a moderate dissipation rate ($\dot{\epsilon} = 0.019\ m/s^3$) and a total biovolume fraction of $\phi = 10^{-4}$. Lines depict the prediction of the sectional method using an equal fragment hypothesis (dashed) and an erosion hypothesis (solid).

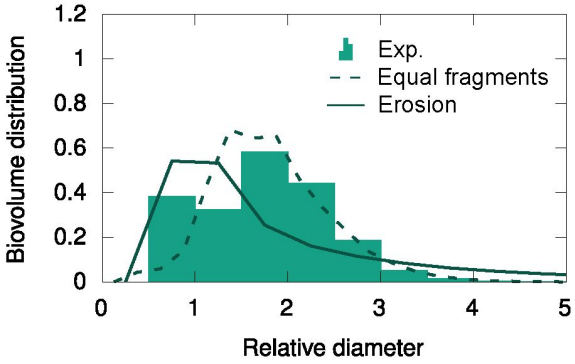

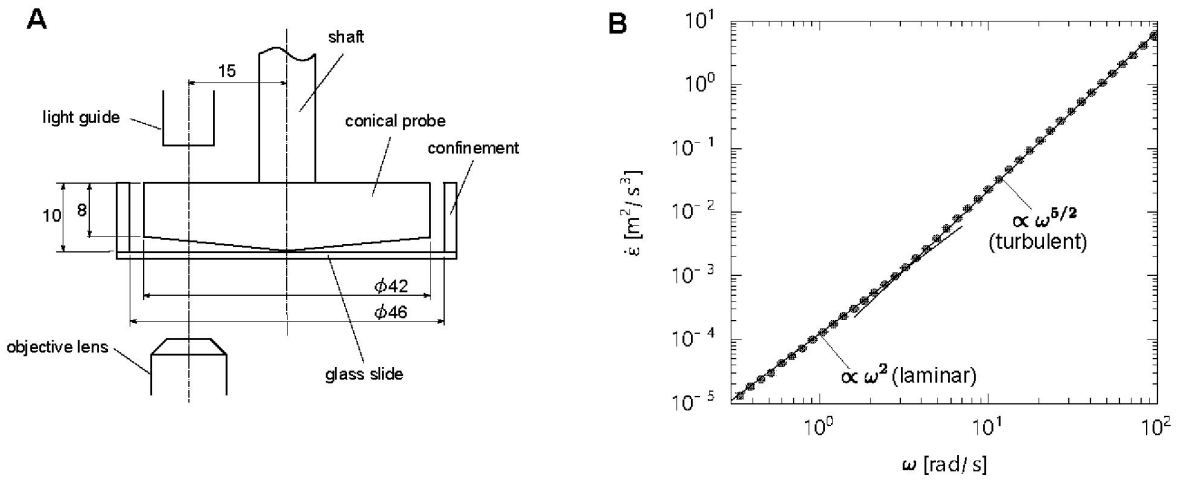

Fig. S7

Cone-and-plate setup used to generate a turbulent shear in a suspension of *Microcystis* colonies. (A) Schematics of the components with the main dimensions indicated in millimeters. (B) Average energy dissipation rate as a function of the angular velocity of the conical probe. Bullets indicate the measured data, and the solid lines indicate the best fit of the laminar regime (~ ω^2) and the inertial regime (~ $\omega^{5/2}$).

References

[1] Stoodley P., Sauer K., Davies D. G., Costerton J. W. (2002) **Biofilms as complex differentiated communities** *Annual Reviews in Microbiology* **56**:187–209

[2] Flemming H.-C., Wingender J. (2010) **The biofilm matrix** *Nature Reviews Microbiology* **8**:623–633

[3] Katharios-Lanwermeyer S., Xi C., Jakubovics N. S., Rickard A. H. (2014) **Mini-review: microbial coaggregation: ubiquity and implications for biofilm development** *Biofouling* **30**:1235–1251

[4] Trunk T., Khalil H. S., Leo J. C. (2018) **Bacterial autoaggregation** *AIMS microbiology* **4**

[5] Martinez-Calvo A., Bhattacharjee T., Bay R. K., Luu H. N., Hancock A. M., Wingreen N. S., Datta S. S. (2022) **Morphological instability and roughening of growing 3d bacterial colonies** *Proceedings of the National Academy of Sciences* **119**

[6] Burd A. B., Jackson G. A. (2009) **Particle aggregation** *Annual Review of Marine Science* **1**:65–90

[7] Drescher K., Shen Y., Bassler B. L., Stone H. A. (2013) **Biofilm streamers cause catastrophic disruption of flow with conse quences for environmental and medical systems** *Proceedings of the National Academy of Sciences* **110**:4345–4350

[8] Rusconi R., Guasto J. S., Stocker R. (2014) **Bacterial transport suppressed by fluid shear** *Nature Physics* **10**:212–217

[9] Rusconi R., Garren M., Stocker R. (2014) **Microfluidics expanding the frontiers of microbial ecology** *Annual Review of Biophysics* **43**:65–91

[10] Atis S., Weinstein B. T., Murray A. W., Nelson D. R. (2019) **Microbial range expansions on liquid substrates** *Physical Review X* **9**

[11] Huisman J., Codd G. A., Paerl H. W., Ibelings B. W., Verspagen J. M. H., Visser P. M. (2018) **Cyanobacterial blooms** *Nature Reviews Microbiology* **16**:471–483

[12] Paerl H. W., Huisman J. (2009) **Climate change: a catalyst for global expansion of harmful cyanobacterial blooms** *Environmental Microbiology Reports* **1**:27–37

[13] Visser P. M., Verspagen J. M. H., Sandrini G., Stal L. J., Matthijs H. C. P., Davis T. W., Paerl H. W., Huisman J. (2016) **How rising CO2 and global warming may stimulate harmful cyanobacterial blooms** *Harmful Algae* **54**:145–159

[14] O'Neil J. M., Davis T. W., Burford M. A., Gobler C. J. (2012) **The rise of harmful cyanobacteria blooms: the potential roles of eutrophication and climate change** *Harmful Algae* **14**:313–334

[15] Ho J. C., Michalak A. M., Pahlevan N. (2019) **Widespread global increase in intense lake phytoplankton blooms since the 1980s** *Nature* **574**:667–670

[16] Ibelings B. W., Bormans M., Fastner J., Visser P. M. (2016) **CYANOCOST special issue on cyanobacterial blooms: synopsis—a critical review of the management options for their prevention, control and mitigation** *Aquatic Ecology* **50**:595–605

[17] Xiao M., Li M., Reynolds C. S. (2018) **Colony formation in the cyanobacterium Microcystis** *Biological Reviews* **93**

[18] Harke M. J., Steffen M. M., Gobler C. J., Otten T. G., Wilhelm S. W., Wood S. A., Paerl H. W. (2016) **A review of the global ecology, genomics, and biogeography of the toxic cyanobacterium, Microcystis spp** *Harmful Algae* **54**:4–20

[19] Visser P. M., Passarge J., Mur L. R. (1997) **Modelling vertical migration of the cyanobacterium Microcystis** *Hydrobiologia* **349**:99–109

[20] Huisman J., Sharples J., Stroom J. M., Visser P. M., Kardinaal W. E. A., Verspagen J. M. H., Sommeijer B. (2004) **Changes in turbulent mixing shift competition for light between phytoplankton species** *Ecology* **85**:2960–2970

[21] Visser P. M., Ibelings B. W., Bormans M., Huisman J. (2016) **Artificial mixing to control cyanobacterial blooms: a review** *Aquatic Ecology* **50**:423–441

[22] Van Le V., Srivastava A., Ko S.-R., Ahn C.-Y., Oh H.-M. (2022) **Microcystis colony formation: extracellular polymeric substance, associated microorganisms, and its application** *Bioresource Technology* **360**

[23] Liu L., Huang Q., Qin B. (2018) **Characteristics and roles of Microcystis extracellular polymeric substances (EPS) in cyanobacterial blooms: a short review** *Journal of Freshwater Ecology* **33**:183–193

[24] Via-Ordorika L., Fastner J., Kurmayer R., Hisbergues M., Dittmann E., Komarek J., Erhard M., Chorus I. (2004) **Distribution of microcystin-producing and non-microcystin-producing Microcystis sp. in european freshwater bodies: detection of microcystins and microcystin genes in individual colonies** *Systematic and Applied Microbiology* **27**:592–602

[25] Perez-Carrascal O. M., Tromas N., Terrat Y., Moreno E., Giani A., Marques L. Correa Braga, Fortin N., Shapiro B. J. (2021) **Single-colony sequencing reveals microbe-by-microbiome phylosymbiosis between the cyanobacterium Microcystis and its associated bacteria** *Microbiome* **9**:1–21

[26] Xiao M., Willis A., Burford M. A., Li M. (2017) **Review: a meta-analysis comparing cell-division and cell-adhesion in Microcystis colony formation** *Harmful Algae* **67**:85–91

[27] Van Leussen W. (1988) **Aggregation of particles, settling velocity of mud flocs a review** *Physical processes in estuaries* :347–403

[28] Kiørboe T., Hansen J. L. S. (1993) **Phytoplankton aggregate formation: observations of patterns and mechanisms of cell sticking and the significance of exopolymeric material** *Journal of Plankton Research* **15**:993–1018

[29] Verspagen J. M. H., Visser P. M., Huisman J. (2006) **Aggregation with clay causes sedimentation of the buoyant cyanobacteria Microcystis spp** *Aquatic Microbial Ecology* **44**:165–174

[30] Day T. C., Marquez-Zacarias P., Bravo P., Pokhrel A. R., MacGillivray K. A., Ratcliff W. C., Yunker P. J. (2022) **Varied solutions to multicellularity: the biophysical and evolutionary consequences of diverse intercellular bonds** *Biophysics Reviews* **3** https://doi.org/10.1063/5.0080845

[31] Feng G., Zhu W., Xue Z., Hu S., Wang R., Zhao S., Chen H. (2020) **Structural variations increase the upper limit of colony size of Microcystis: implications from laboratory cultures and field investigations** *Journal of Phycology* **56**:1676–1686

[32] Li M., Xiao M., Zhang P., Hamilton D. P. (2018) **Morphospecies-dependent disaggregation of colonies of the cyanobacterium Microcystis under high turbulent mixing** *Water Research* **141**:340–348

[33] Wilkinson A., Hondzo M., Guala M., et al. (2016) **Effect of small-scale turbulence on the growth and metabolism of Microcystis aeruginosa** *Advances in Microbiology* **6**

[34] Xiao Y., Li Z., Li C., Zhang Z., Guo J. (2016) **Effect of small-scale turbulence on the physiology and morphology of two bloom-forming cyanobacteria** *PloS One* **11**

[35] Medrano E. A., Uittenbogaard R. E., Pires L. M. D., Van De Wiel B. J. H., Clercx H. J. H. (2013) **Coupling hydrodynamics and buoyancy regulation in Microcystis aeruginosa for its vertical distribution in lakes** *Ecological Modelling* **248**:41–56

[36] Rowe M. D., Anderson E. J., Wynne T. T., Stumpf R. P., Fanslow D. L., Kijanka K., Vanderploeg H. A., Strickler J. R., Davis T. W. (2016) **Vertical distribution of buoyant Microcystis blooms in a lagrangian particle tracking model for short-term forecasts in lake erie** *Journal of Geophysical Research: Oceans* **121**:5296–5314

[37] Ranjbar M. H., Hamilton D. P., Etemad-Shahidi A., Helfer F. (2021) **Individual-based modelling of cyanobacteria blooms: physical and physiological processes** *Science of the Total Environment* **792**

[38] Nakamura T., Adachi Y., Suzuki M. (1993) **Flotation and sedimentation of a single Microcystis floc collected from surface bloom** *Water Research* **27**:979–983

[39] O'Brien K. R., Meyer D. L., Waite A. M., Ivey G. N., Hamilton D. P. (2004) **Disaggregation of Microcystis aeruginosa colonies under turbulent mixing: laboratory experiments in a grid-stirred tank** *Hydrobiologia* **519**:143–152

[40] Lai C. C. K., Socolofsky S. A. (2019) **The turbulent kinetic energy budget in a bubble plume** *Journal of Fluid Mechanics* **865**:993–1041

[41] Peter C. P., Suzuki Y., Buchs J. (2006) **Hydromechanical stress in shake flasks: correlation for the maximum local energy dissipation rate** *Biotechnology and Bioengineering* **93**:1164–1176

[42] Flesch J. C., Spicer P. T., Pratsinis S. E. (1999) **Laminar and turbulent shear-induced flocculation of fractal aggregates** *AIChE Journal* **45**:1114–1124

[43] Vankova N., Tcholakova S., Denkov N. D., Vulchev V. D., Danner T. (2007) **Emulsification in turbulent flow: 2. breakage rate constants** *Journal of Colloid and Interface Science* **313**:612–629

[44] Hakansson A. (2020) **Experimental methods for measuring the breakup frequency in turbulent emulsification: a critical review** *ChemEngineering* **4**

[45] Saffman P. G. F., Turner J. S. (1956) **On the collision of drops in turbulent clouds** *Journal of Fluid Mechanics* **1**:16–30

[46] Baebler M. U., Morbidelli M., Baldyga J. (2008) **Modelling the breakup of solid aggregates in turbulent flows** *Journal of Fluid Mechanics* **612**:261–289

[47] Zaccone A., Soos M., Lattuada M., Wu H., Buabler M. U., Morbidelli M. (2009) **Breakup of dense colloidal aggregates under hydrodynamic stresses** *Physical Review E* **79**

[48] Vanni M. (2000) **Approximate population balance equations for aggregation-breakage processes** *Journal of Colloid and Interface Science* **221**:143–160

[49] Kumar S., Ramkrishna D. (1996) **On the solution of population balance equations by discretization—i. a fixed pivot technique** *Chemical Engineering Science* **51**:1311–1332

[50] Byrne E., Dzul S., Solomon M., Younger J., Bortz D. M. (2011) **Postfragmentation density function for bacterial aggregates in laminar flow** *Physical Review E* **83**

[51] Balmforth N. J., Frigaard I. A., Ovarlez G. (2014) **Yielding to stress: recent developments in viscoplastic fluid mechanics** *Annual Review of Fluid Mechanics* **46**:121–146

[52] Bonn D., Denn M. M., Berthier L., Divoux T., Manneville S. (2017) **Yield stress materials in soft condensed matter** *Reviews of Modern Physics* **89**

[53] Grad Y., Einav S. (2000) **Spectral and instantaneous flow field characteristics of the laminar to turbulent transition in a cone and plate apparatus** *Experiments in Fluids* **28**:336–343

[54] Babler M. U. *et al.* (2015) **Numerical simulations of aggregate breakup in bounded and unbounded turbulent flows** *Journal of Fluid Mechanics* **766**:104–128

[55] Xu F., Zhu W., Xiao M., Li M. (2016) **Interspecific variation in extracellular polysaccharide content and colony formation of Microcystis spp. cultured under different light intensities and temperatures** *Journal of Applied Phycology* **28**:1533–1541

[56] Gu P., Li Q., Zhang W., Zheng Z., Luo X. (2020) **Effects of different metal ions (Ca, Cu, Pb, Cd) on formation of cyanobacterial blooms** *Ecotoxicology and Environmental Safety* **189**

[57] Chen H., Luurling M. (2020) **Calcium promotes formation of large colonies of the cyanobacterium Microcystis by enhancing cell-adhesion** *Harmful Algae* **92**

[58] Wang W., Liu Y., Geng L., Yang Z., Chen Y. (2011) **The effect of nitrogen concentration and its interaction with light intensity on population dynamics and polysaccharide content of Microcystis aeruginosa** *Journal of Freshwater Ecology* **26**:241–248

[59] Chorus I., Welker M. (2021) **Toxic cyanobacteria in water: a guide to their public health consequences, monitoring and management** Taylor & Francis

[60] Wuuest A., Lorke A. (2003) **Small-scale hydrodynamics in lakes** *Annual Review of fluid mechanics* **35**:373–412

[61] Wu X., Yang T., Feng S., Li L., Xiao B., Song L., Sukenik A., Ostrovsky I. (2020) **Recovery of Microcystis surface scum following a mixing event: insights from a tank experiment** *Science of the Total Environment* **728**

[62] Wu X., Noss C., Liu L., Lorke A. (2019) **Effects of small-scale turbulence at the air-water interface on Microcystis surface scum formation** *Water Research* **167**

[63] Laufhotte H. D., Mersmann A. (1987) **Local energy dissipation in agitated turbulent fluids and its significance for the design of stirring equipment** *Chemical Engineering & Technology* **10**:56–63

[64] Smith D. J., Tan J. Y., Powers M. A., Lin X. N., Davis T. W., Dick G. J. (2021) **Individual Microcystis colonies harbour distinct bacterial communities that differ by Microcystis oligotype and with time** *Environmental Microbiology* **23**:3020–3036

[65] Goldstein R. E. (2015) **Green algae as model organisms for biological fluid dynamics** *Annual Review of Fluid Mechanics* **47**:343–375

[66] Thomen P., Robert J., Monmeyran A., Bitbol A.-F., Douarche C., Henry N. (2017) **Bacterial biofilm under flow: first a physical struggle to stay, then a matter of breathing** *PloS one* **12**

[67] Ros-Rocher N., Reyes-Rivera J., Foroughijabbari Y., Combredet C., Larson B. T., Coyle M. C., Houtepen E. A. T., Vermeij M. J. A., King N., Brunet T. (2024) **Mixed clonal-aggregative multicellularity entrained by extreme salinity fluctuations in a close relative of animals** :2024–3

[68] Ducat D. C., Way J. C., Silver P. A. (2011) **Engineering cyanobacteria to generate high-value products** *Trends in Biotechnology* **29**:95–103

[69] Parmar A., Singh N. K., Pandey A., Gnansounou E., Madamwar D. (2011) **Cyanobacteria and microalgae: a positive prospect for biofuels** *Bioresource Technology* **102**:10163–10172

[70] Johnson T. J., Katuwal S., Anderson G. A., Gu L., Zhou R., Gibbons W. R. (2018) **Photobioreactor cultivation strategies for microalgae and cyanobacteria** *Biotechnology Progress* **34**:811–827

[71] Kardinaal W. E. A., Tonk L., Janse I., Hol S., Slot P., Huisman J., Visser P. M. (2007) **Competition for light between toxic and nontoxic strains of the harmful cyanobacterium Microcystis** *Applied and Environmental Microbiology* **73**:2939–2946

[72] Humphries S. E., Widjaja F. (1979) **A simple method for separating cells of Microcystis aeruginosa for counting** *British Phycological Journal* **14**:313–316

[73] Buschmann M. H., Dieterich P., Adams N. A., Schnittler H. .-. (2005) **Analysis of flow in a cone-and-plate apparatus with respect to spatial and temporal effects on endothelial cells** *Biotechnology and Bioengineering* **89**:493–502

[74] Ye C., Ali S., Sun Q., Guo M., Liu Y., Gao Y., Huo B. (2019) **Novel cone-and-plate flow chamber with controlled distribution of wall fluid shear stress** *Computers in Biology and Medicine* **106**:140–148

[75] Van der Walt S., Schonberger J. L., Nunez-Iglesias J., Boulogne F., Warner J. D., Yager N., Gouillart E., Yu T. (2014) **Scikit-image: image processing in python** *PeerJ* **2**

[76] Gao F., Han L. (2012) **Implementing the nelder-mead simplex algorithm with adaptive parameters** *Computational Optimization and Applications* **51**:259–277

[1] Burd A. B., Jackson G. A. (2009) **Particle aggregation** *Annual Review of Marine Science* **1**:65–90

[2] Saffman P. G. F., Turner J. S. (1956) **On the collision of drops in turbulent clouds** *Journal of Fluid Mechanics* **1**:16–30

[3] Sdougos H. P., Bussolari S. R., Dewey C. F. (1984) **Secondary flow and turbulence in a cone-and-plate device** *Journal of Fluid Mechanics* **138**:379–404

[4] Grad Y., Einav S. (2000) **Spectral and instantaneous flow field characteristics of the laminar to turbulent transition in a cone and plate apparatus** *Experiments in Fluids* **28**:336–343

Author information

Yuri Z Sinzato
Van der Waals-Zeeman Institute, Institute of Physics, University of Amsterdam, Amsterdam, The Netherlands
ORCID iD: 0000-0002-3324-5712

For correspondence: y.z.smzato@uva.nl

Robert Uittenbogaard
Hydro-Key Ltd, Haelen, The Netherlands

Petra M Visser
Department of Freshwater and Marine Ecology, Institute for Biodiversity and Ecosystem Dynamics, University of Amsterdam, Amsterdam, The Netherlands

Jef Huisman
Department of Freshwater and Marine Ecology, Institute for Biodiversity and Ecosystem Dynamics, University of Amsterdam, Amsterdam, The Netherlands

Maziyar Jalaal
Van der Waals-Zeeman Institute, Institute of Physics, University of Amsterdam, Amsterdam, The Netherlands
ORCID iD: 0000-0002-5654-8505

For correspondence: m.jalaal@uva.nl

Editors

Reviewing Editor
Babak Momeni
Boston College, Chestnut Hill, United States of America

Senior Editor
Felix Campelo
Institute of Photonic Sciences, Barcelona, Spain

Reviewer #1 (Public review):

This work has significant relevance to the field, both practically and naturally. Combatting or preventing toxic cyanobacterial blooms is an active area of environmental research that offers a practical backbone for this manuscript's ideas. Additionally, the formation and behavior of cellular aggregates, in general, is of widespread interest in many fields, including marine and freshwater ecology, healthcare and antibiotic resistance research, biophysics, and microbial evolution. In this field, there are still outstanding questions regarding how microbial aggregates form into communities, including if and how they come together from separate places. Therefore, I believe that researchers from many distinct fields would find interest in the topic of this paper, particularly Figure 5, in which a phase space that is meant to represent the different modes of aggregate formation and destruction is suggested, dependent on properties of the fluid flow and particle concentration.

Altogether, the authors were mostly successful in their investigation, and I find most of their claims to be justified. In particular, the authors achieve strong results from their experiments regarding aggregate fragmentation. However, readers could benefit from some clarification in a couple of key areas. Additionally, I found that some of the authors' claims were based on weak or nonexistent data. Below, I outline the key claims of the paper and indicate the level to which they were supported by their data.

- Their first major claim is that fluid flows alone must be quite strong in order to fragment the cyanobacterial aggregates they have studied. With their rheological chamber, they explicitly show that energy dissipation rates must exceed "natural" conditions by multiple orders of magnitude in order to fragment lab strain colonies, and even higher to disrupt natural strains sampled from a nearby freshwater lake. This claim is well-supported by their experiments and data.
- The authors then claim that the fragmentation of aggregates due to fluid flows occurs through erosion of small pieces. Because their experimental setup does not allow them to explicitly observe this process (for example, by watching one aggregate break into pieces), they implement an idealized model to show that the nature of the changes to the size histogram agrees with an erosion process. However, in Figure 2C there is a noticeable gap between their experiment and the prediction of their model. Additionally, in a similar experiment shown in Figure S6, the experiment cannot distinguish between an idealized erosion model and an alternative, an idealized binary fission model where aggregates split into equal halves. For these reasons, this claim is weakened.
- Their third major claim is that fluid flows only weakly cause cells to collide and adhere in a "coming together" process of aggregate formation. They test this claim in Figure 3, where they suspend single cells in their test chamber and stir them at moderate intensity, monitoring their size histogram. They show that the size histogram changes only slightly, indicating that aggregation is, by and large, not occurring at a high rate. Therefore, they lend support to the idea that cell aggregation likely does not initiate group formation in toxic cyanobacterial blooms. Additionally, they show that the median size of large colonies also does not change at moderate turbulent intensities. These results agree with previous studies (their own citation 25) indicating that aggregates in toxic blooms are clonal in nature. This is an important result and well-supported by their data, but only for this specific particle concentration and stirring intensity. Later, in Figure 5 they show a much broader range of particle concentrations and energy dissipation rates that they leave untested.
- The fourth major result of the manuscript is displayed in Equation 8 and Figure 5, where the authors derive an expression for the ratio between the rate of increase of a colony due to aggregation vs. the rate due to cell division. They then plot this line on a phase map, altering two physical parameters (concentration and fluid turbulence) to show under what conditions aggregation vs. cell division are more important for group formation. Because these results are derived from relatively simple biophysical considerations, they have the potential to be

quite powerful and useful and represent a significant conceptual advance. However, there is a region of this phase map that the authors have left untested experimentally. The lowest energy dissipation rate that the authors tested in their experiment seemed to be \dot{epsilon}~1e-2 [m^2/s^3], and the highest particle concentration they tested was 5e-4, which means that the authors never tested Zone II of their phase map. Since this seems to be an important zone for toxic blooms (i.e. the "scum formation" zone), it seems the authors have missed an important opportunity to investigate this regime of high particle concentrations and relatively weak turbulent mixing.

Other items that could use more clarity:
- The authors rely heavily on size distributions to make the claims of their paper. Yet, how they generated those size distributions is not clearly shown in the text. Of primary concern, the authors used a correction function (Equation S1) to estimate the counts of different size classes in their image analysis pipeline. Yet, it is unclear how well this correction function actually performs, what kinds of errors it might produce, and how well it mapped to the calibration dataset the authors used to find the fit parameters.
- Second, in their models they use a fractal dimension to estimate the number of cells in the group from the group radius, but the agreement between this fractal dimension fit and the data is not shown, so it is not clear how good an approximation this fractal dimension provides. This is especially important for their later derivation of the "aggregation-to-cell division" ratio (Equation 8).

https://doi.org/10.7554/eLife.103503.1.sa2

Reviewer #2 (Public review):

Summary:

In this work, the authors investigate the role of fluid flow in shaping the colony size of a freshwater cyanobacterium Microcystis. To do so, they have created a novel assay by combining a rheometer with a bright field microscope. This allows them to exert precise shear forces on cyanobacterial cultures and field samples, and then quantify the effect of these shear forces on the colony size distribution. Shear force can affect the colony size in two ways: reducing size by fragmentation and increasing size by aggregation. They find limited aggregation at low shear rates, but high shear forces can create erosion-type fragmentation: colonies do not break in large pieces, but many small colonies are sheared off the large colonies. Overall, bacterial colonies from field samples seem to be more inert to shear than laboratory cultures, which the authors explain in terms of enhanced intercellular adhesion mediated by secreted polysaccharides.

Strengths:

-This study is timely, as cyanobacterial blooms are an increasing problem in freshwater lakes. They are expected to increase in frequency and severeness because of rising temperatures, and it is worthwhile learning how these blooms are formed. More generally, how physical aspects such as flow and shear influence colony formation is often overlooked, at least in part because of experimental challenges. Therefore, the method developed by the authors is useful and innovative, and I expect applications beyond the presented system here.
-A strong feature of this paper is the highly quantitative approach, combining theory with experiments, and the combination of laboratory experiments and field samples.

Weaknesses:

-Especially the introduction seems to imply that shear force is a very important parameter controlling colony formation. However, if one looks at the results this effect is overall rather

modest, especially considering the shear forces that these bacterial colonies may experience in lakes. The main conclusion seems that not shear but bacterial adhesion is the most important factor in determining colony size. As the importance of adhesion had been described elsewhere, it is not clear what this study reveals about cyanobacterial colonies that was not known before.
-The agreement between model and experiments is impressive, but the role of the fit parameters in achieving this agreement needs to be further clarified.
-The article may not be very accessible for readers with a biology background. Overall, the presentation of the material can be improved by better describing their new method.

https://doi.org/10.7554/eLife.103503.1.sa1

Author response:

We thank the reviewers and the editor for the detailed and constructive feedback provided. We look forward to submitting a revised version of the manuscript that addresses their comments. We acknowledge that further clarification is needed about the novelty brought by our experimental setup and model in comparison to previous studies using different methodologies. We also acknowledge that more details can be included about the calibration steps and sensitivity of the model parameters. Below we detail the planned changes for the revised version regarding the points raised by the reviewers.

> ***Reviewer #1 (Public review):***
>
> *- The authors then claim that the fragmentation of aggregates due to fluid flows occurs through erosion of small pieces. Because their experimental setup does not allow them to explicitly observe this process (for example, by watching one aggregate break into pieces), they implement an idealized model to show that the nature of the changes to the size histogram agrees with an erosion process. However, in Figure 2C there is a noticeable gap between their experiment and the prediction of their model. Additionally, in a similar experiment shown in Figure S6, the experiment cannot distinguish between an idealized erosion model and an alternative, an idealized binary fission model where aggregates split into equal halves. For these reasons, this claim is weakened.*

The two idealized models of fragment distribution, namely erosion and binary fission, lead to distinguishable final size distributions. We believe that our experiments support the hypothesis of the erosion mechanism. Please note that Figure 2 is concerned with the fragmentation of large colonies, whereas Figure 3 and associated Figure S6 are concerned with very small colonies of a few cells formed by aggregation of single-cell suspension. Indeed, for very small colonies of a few cells, our experimental results cannot distinguish between a binary fission model and an erosion model (Figure S6).

The situation is very different for large colonies. To address the reviewer's concern, we will add a new figure in the Supplementary Information (SI), similar to our Figure 2C, where we will compare the erosion model with a binary fission model for large colonies fragmented under $\varepsilon = 5.8\ m^2/s^3$. We already did this exercise. The results in this new supplementary figure will show that the idealized binary fission model (i.e., where every fracture event produces exactly two fragments) does not capture the experimental fragmentation behaviour of large colonies. In contrast, the idealized erosion model provides a much better prediction of the experimental results, within the experimental uncertainty and variability in colony strength, and has the notable advantage of a straightforward computational implementation.

> *- The fourth major result of the manuscript is displayed in Equation 8 and Figure 5, where the authors derive an expression for the ratio between the rate of increase of a*

> *colony due to aggregation vs. the rate due to cell division. They then plot this line on a phase map, altering two physical parameters (concentration and fluid turbulence) to show under what conditions aggregation vs. cell division are more important for group formation. Because these results are derived from relatively simple biophysical considerations, they have the potential to be quite powerful and useful and represent a significant conceptual advance. However, there is a region of this phase map that the authors have left untested experimentally. The lowest energy dissipation rate that the authors tested in their experiment seemed to be \dot{epsilon}~1e-2 [m^2/s^3], and the highest particle concentration they tested was 5e-4, which means that the authors never tested Zone II of their phase map. Since this seems to be an important zone for toxic blooms (i.e. the "scum formation" zone), it seems the authors have missed an important opportunity to investigate this regime of high particle concentrations and relatively weak turbulent mixing.*

We agree with the reviewer that Zone (II) of Figure 5 is of great importance to dense bloom formation under wind mixing and that this parameter range was not covered by our experiments using a cone-and-plate shear flow. The measuring range of our device was motivated by engineering applications such artificial mixing of eutrophic lakes using bubble plumes, as well as preliminary experiments which demonstrated that high levels of dissipation rate were required to achieve fragmentation. The dissipation rates of our cone-and-plate experiments capture Zones (III) and (IV) and the higher end of Zone (I). However, the cone-and-plate experiments are less suitable for the lower dissipation rates of Zone (II), as indicated by the red bars in Figure 5, due to the accumulation of colonies in stagnation points.

Instead, in our revision we will more extensively discuss recent results published in the literature for evidence of aggregation-dominance at Zone (II). The experimental studies of Wu et al. (2019) and Wu et al. (2024) (full citation below) investigated the formation of *Microcystis* surface scum layers at high colony concentrations (high biovolume fraction) in wind-mixed mesocosms. These studies identified aggregation of colonies at rates faster than cell division, while the stable colony size decreased with mixing rate. The parameter range of these studies fall within Zone II, and their experimental results agree with our model predictions. We will include in the reviewed version these references and a detailed discussion elucidating the parameter range covered in our experiments and the findings of other studies.

Wu, X., Noss, C., Liu, L., & Lorke, A. (2019). Effects of small-scale turbulence at the air-water interface on *Microcystis* surface scum formation. *Water Research*, *167*, 115091.

Wu, H., Wu, X., Rovelli, L., & Lorke, A. (2024). Dynamics of Microcystis surface scum formation under different wind conditions: the role of hydrodynamic processes at the air-water interface. Frontiers in Plant Science, 15, 1370874.

> *Other items that could use more clarity:*
>
> *- The authors rely heavily on size distributions to make the claims of their paper. Yet, how they generated those size distributions is not clearly shown in the text. Of primary concern, the authors used a correction function (Equation S1) to estimate the counts of different size classes in their image analysis pipeline. Yet, it is unclear how well this correction function actually performs, what kinds of errors it might produce, and how well it mapped to the calibration dataset the authors used to find the fit parameters.*

We agree with the reviewer that more details of the calibration processes should be included. We will include in the revised version of the SI more details of the calibration steps and direct comparison of raw and corrected histograms of the size distribution and its associated uncertainty.

> *- Second, in their models they use a fractal dimension to estimate the number of cells in the group from the group radius, but the agreement between this fractal dimension fit and the data is not shown, so it is not clear how good an approximation this fractal dimension provides. This is especially important for their later derivation of the "aggregation-to-cell division" ratio (Equation 8)*

We agree with the reviewer that more details on the estimation of fractal dimension are needed. The revised version of the SI will include the estimation procedure, the number of colonies analysed, and the associated uncertainty.

> ***Reviewer #2 (Public review)***
>
> *- Especially the introduction seems to imply that shear force is a very important parameter controlling colony formation. However, if one looks at the results this effect is overall rather modest, especially considering the shear forces that these bacterial colonies may experience in lakes. The main conclusion seems that not shear but bacterial adhesion is the most important factor in determining colony size. As the importance of adhesion had been described elsewhere, it is not clear what this study reveals about cyanobacterial colonies that was not known before.*

As we explain in the Introduction, it is a major open question whether cyanobacterial colonies are formed mainly by cell division (after which the dividing cells remain attached to each other by the EPS layer) or mainly by the aggregation of independent cells & colonies. See for example the highly cited review of Xiao & Reynolds 2018 (our ref 17), and references therein. This question has not been resolved and is investigated in our study. We would like to emphasize several key findings that our study reveals about the mechanical behaviour of cyanobacterial colonies under flow:

(i) Quantification of mechanical strength in cyanobacterial colonies: Our results demonstrate the high mechanical strength of cyanobacterial colonies (much higher than previously thought in references 32 and 39 of the manuscript), as evidenced by the requirement of very high shear rates to achieve fragmentation. To this end, our study highlights their resilience against naturally occurring flows and bridges the gap between theoretical assumptions about colony strength and experimentally measured mechanical properties.

(ii) Validation of a hypothesis regarding colony formation: Using a fluid-mechanical approach, we confirm the findings of recent genetic studies (references 25 and 64 of the manuscript) which indicated that colony formation of cyanobacteria under natural conditions occurs predominantly via cell division rather than via the aggregation of individual cells. Only in very dense blooms and surface scums, colony formation by the aggregation of smaller colonies likely plays a role.

(iii) Practical guidelines for cyanobacterial bloom control: Our findings provide valuable insights into the design of artificial mixing systems that are used to suppress surface blooms of buoyant cyanobacteria in lakes. In these lake applications, in which we have been involved, the aim of the mixing is to disperse the colonies over the water column so that they cannot form a surface layer (i.e., the mixing intensity should overcome the flotation velocity of the colonies), which takes away the competitive advantage of buoyant cyanobacteria over nonbuoyant phytoplankton species. However, it has always been an open question whether the high shear of artificial mixing would cause colony fragmentation. An understanding of changes in colony size is relevant for the design of artificial mixing, because smaller colonies have a lower flotation velocity. Our results show that the dissipation rates that are generated by artificial mixing are sufficient to prevent aggregation of large colonies, but not high enough to induce fragmentation of division-formed colonies.

In the revised version of the manuscript, we will improve the writing to better clarify these three novel insights obtained from our study.

> *- The agreement between model and experiments is impressive, but the role of the fit parameters in achieving this agreement needs to be further clarified.*

The influence of the fit parameters (namely the stickiness $\alpha 1$ and the pairs of colony strength parameters $S1,q1,S2,q2$) is discussed in the sections “DYNAMICAL CHANGES IN COLONY SIZE MODELED BY A TWO-CATEGORY DISTRIBUTION” and “MATERIALS AND METHODS.” We kept the discussion concise to maintain readability. However, we agree with the reviewer that additional details about the importance of the fit parameters and the sensitivity of the results to these parameters could be beneficial. In the revised version of the SI, we will include a more detailed discussion of the fit parameters.

> *- The article may not be very accessible for readers with a biology background. Overall, the presentation of the material can be improved by better describing their new method.*

We apologize for the limited readability of the description of the experimental setup and model used. In the revised version of the manuscript, we aim to expand the description of the new methods presented here for a broader audience of biology.

https://doi.org/10.7554/eLife.103503.1.sa0